GABAergic Contributions to Gating, Timing, and Phase Precession of Hippocampal Neuronal Activity During Theta Oscillations

Vassilis Cutsuridis*[1] and Michael Hasselmo[2]

ABSTRACT: Successful spatial exploration requires gating, storage, and retrieval of spatial memories in the correct order. The hippocampus is known to play an important role in the temporal organization of spatial information. Temporally ordered spatial memories are encoded and retrieved by the firing rate and phase of hippocampal pyramidal cells and inhibitory interneurons with respect to ongoing network theta oscillations paced by intra- and extrahippocampal areas. Much is known about the anatomical, physiological, and molecular characteristics as well as the connectivity and synaptic properties of various cell types in the hippocampal microcircuits, but how these detailed properties of individual neurons give rise to temporal organization of spatial memories remains unclear. We present a model of the hippocampal CA1 microcircuit based on observed biophysical properties of pyramidal cells and six types of inhibitory interneurons: axo-axonic, basket, bistratistified, neurogliaform, ivy, and oriens lacunosum-moleculare cells. The model simulates a virtual rat running on a linear track. Excitatory transient inputs come from the entorhinal cortex (EC) and the CA3 Schaffer collaterals and impinge on both the pyramidal cells and inhibitory interneurons, whereas inhibitory inputs from the medial septum impinge only on the inhibitory interneurons. Dopamine operates as a gate-keeper modulating the spatial memory flow to the PC distal dendrites in a frequency-dependent manner. A mechanism for spike-timing-dependent plasticity in distal and proximal PC dendrites consisting of three calcium detectors, which responds to the instantaneous calcium level and its time course in the dendrite, is used to model the plasticity effects. The model simulates the timing of firing of different hippocampal cell types relative to theta oscillations, and proposes functional roles for the different classes of the hippocampal and septal inhibitory interneurons in the correct ordering of spatial memories as well as in the generation and maintenance of theta phase precession of pyramidal cells (place cells) in CA1. The model leads to a number of experimentally testable predictions that may lead to a better understanding of the biophysical computations in the hippocampus and medial septum. © 2012 Wiley Periodicals, Inc.

KEY WORDS: computer model; hippocampus; inhibitory interneurons; STDP; dopamine

INTRODUCTION

Episodic memory is the memory of autobiographical events at specific times and places. For example, returning home by car from a new destination requires remembering a spatiotemporal trajectory through specific streets including a sequence of landmarks at different positions. The hippocampus is a key brain structure known to link spatial memories (e.g. landmarks) together in a sequential manner across time. Retrieving these spatial memories in the correct order is instrumental if one wants to return home on time for dinner.

The encoding and retrieval of spatiotemporal sequences may involve the activity of pyramidal cells (place cells) in the hippocampus. The firing rate and phase of place cells changes with respect to theta oscillations (O'Keefe and Recce, 1993; Wilson et al., 1993; Skaggs et al., 1996; Johnson and Redish, 2007). Theta oscillations (4–10 Hz) are observed during exploration in animals and rapid eye movement sleep (Buzsaki, 2002). During exploration hippocampal place cells have been shown to systematically shift their phase of firing to earlier phases of the theta rhythm as the animal transverses the place field (a phenomenon known as theta phase precession) (O'Keefe and Recce, 1993; Skaggs et al., 1996).

In recent years an expansion of knowledge about the anatomical, physiological, and molecular characteristics as well as the connectivity and synaptic properties of the various cell types in the hippocampal microcircuits has occurred (Cutsuridis et al., 2010). Pyramidal cells (PCs) in region CA1 receive inputs through the perforant path from layer III of the entorhinal cortex (EC) in their distal dendrites and from the CA3 Schaffer collaterals as a portion of the trisynaptic loop to their proximal dendrites. The effects of these inputs in the distal and proximal dendrites are also subject to effects of neuromodulators such as dopamine and acetylcholine (Cobb and Lawrence, 2010). The effects of dopamine have been shown to be location- (Otmakhova and Lisman, 1999) and frequency-dependent (Ito and Schumann, 2007). When DA is applied to a bathing solution, the field-EPSP evoked by the EC stimulation is depressed, whereas the fEPSP by the CA3 Schaffer collateral (SC) pathway stimulation remains unaltered (Otmakhova and Lisman, 1999). A recent study by Ito and Schuman (2007) showed DA to act as a gate on the EC cortical input to the CA1 PC distal dendrites, modulating the information flow and the synaptic plasticity in a frequency-dependent manner. PCs in region CA1 have been theorized to compare the inputs from EC and

CA3 to detect either novelty (Vinogradova, 2001), mismatch of expectations (Hasselmo and Schnell, 1994), or activation of retrieval mechanisms (Lee and Kesner, 2004).

At least 21 different types of inhibitory interneurons have been identified in region CA1 of the hippocampus (Klausberger et al., 2005; Somogyi and Klausberger, 2005; Jinno et al., 2007; Fuentealba et al., 2008a,b, 2010). These cells are distinguished based on their anatomical, morphological, pharmacological, and physiological properties (Ascoli et al., 2008). These include the axo-axonic cells (AAC), the perisomatic basket cells (BC) and the dendritic bistratified (BSC), ivy (IVY), neuroglia-form (NGL) and oriens lacunosum-moleculare (OLM) cells (Somogyi and Klausberger, 2005; Fuentealba et al., 2008). AACs innervate exclusively the initial axonal segment of the CA1 PC, whereas BCs innervate their cell bodies and proximal dendrites (Somogyi and Klausberger, 2005). BSCs and IVYs innervate the PC basal and oblique dendrites, whereas OLM and NGL cells target the apical dendritic tuft of PCs aligned with the EC input (Somogyi and Klausberger, 2005; Fuentealba et al., 2008; Capogna, 2011). AACs and BCs receive excitatory inputs from both the EC and the CA3 Schaffer collaterals, whereas the BSCs receive inputs only from CA3 and the NGLs only from the EC (Somogyi and Klausberger, 2005; Capogna, 2011). IVYs and OLMs are recurrently excited by the CA1 PCs (Somogyi and Klausberger, 2005; Fuentealba et al., 2008a,b).

PCs, AACs, BCs, BSCs, IVYs, NGLs, and OLMs have been shown to display diverse firing patterns during network oscillations (Klausberger and Somogyi, 2008; Fuentealba et al., 2008a,b, 2010; Cobb and Vida, 2010). The firing patterns of inhibitory interneurons may have different functional roles (Cutsuridis, Cobb and Graham, 2010). For example, gamma oscillations constitute a basic clock and have been linked to a variety of cognitive phenomena (Colgin et al., 2009). Gamma oscillations in region CA1 of the hippocampus split into distinct fast and slow frequency components that differentially couple CA1 to inputs from the medial entorhinal cortex (fast) and the CA3 (slow) (Colgin et al., 2009). A computational study by Hasselmo and colleagues (2002) showed theta oscillations to be involved in memory formation by phasing encoding and retrieval in different functional sub-cycles of theta. Experimental evidence has shown that during theta oscillations OLMs, BSCs, IVYs and PCs fire at the trough of theta recorded in stratum pyramidale, whereas AACs, BCs and NGLs fire at the peak of theta (Klausberger and Somogyi, 2008; Fuentealba et al., 2008a,b, 2010). Cutsuridis et al. (2008, 2009, 2010) were the first to demonstrate the biological feasibility of the separation of storage and recall processes into separate theta subcycles while suggesting functional roles for the theta modulated AAC, BC, BSC, and OLM cells. According to these computational studies (Cutsuridis et al., 2008, 2009, 2010) during the encoding process AACs and BCs exert powerful inhibitory control to PCs, which prevents them from firing and the information from "leaking out." During the retrieval process BSC inhibition is needed for accurate recall of a previously stored pattern by contributing to the thresholding of

pyramidal cell firing, whereas OLM inhibition is effective at removing spurious EC input which may interfere with pattern recall.

Theta rhythm in the hippocampus has been shown to be paced by the medial septal (MS) GABAergic neurons (Winson, 1978; Vertes and Kocsis, 1997). The MS and the hippocampus are reciprocally connected (Toth et al., 1993). The parvalbumin-immunoreactive GABAergic neurons of MS (Freund, 1989), have been shown to selectively innervate GABAergic interneurons in the hippocampus (Freund and Antal, 1988), which in turn project back to MS and inhibit the MS GABAergic neurons (Toth et al., 1993). GABAergic MS neurons form two distinct populations exhibiting highly regular bursting activity that is coupled to either the trough or the peak of hippocampal theta waves (Borhegyi et al., 2004).

Cutsuridis et al. (2008, 2009) were the first to introduce a detailed biophysical model of the CA1 microcircuit in order to investigate how storage and recall are controlled in CA1 in the presence of various inhibitory interneurons and as a function of input pattern loading and presentation frequency. The neuronal diversity, morphology, ionic, and synaptic properties, connectivity, and spatial distribution closely followed known experimental evidence of the hippocampal microcircuitry (Cutsuridis et al., 2010). In a subsequent modeling study, Cutsuridis et al. (2010) extended the model of the CA1 microcircuitry to test its recall performance of new and previously stored *static* patterns as well as its memory capacity in the presence/absence of various inhibitory interneurons.

In this article, we extended these models and investigated how gating, encoding, and retrieval of spatial memories in the correct order are achieved by the CA1 pyramidal cells during theta oscillations in the presence of different forms of hippocampal and septal inhibition. In contrast to previous models (Cutsuridis et al., 2008, 2010; Cutsuridis and Wennekers, 2009), our model used simplified morphologies of pyramidal cells and inhibitory interneurons. Our network consisted of an AAC, a BC, a BSC, an OLM, four IVYs, and four NGLs (see Fig. 1). Distal and proximal dendrites of the PCs were excited by EC perforant path and CA3 Schaffer collateral inputs (Witter, 2010). Hippocampal inhibitory interneurons were inhibited by MS inputs (Freund and Antal, 1988). Excitatory and inhibitory inputs to PC distal dendrites were modulated by dopamine (DA), which acted as a gate-keeper opening and closing the gate in the PC distal dendrites in a frequency-dependent manner (Ito and Schumann, 2007). Plasticity effects in the distal and proximal PC dendrites were measured via a mechanism for spike-timing-dependent plasticity (STDP), which responded to the instantaneous calcium level and its time course in the dendrite (see Fig. 2). Our model simulated accurately the timing of firing of different hippocampal cell types relative to theta oscillations (Borhegyi et al., 2004; Klausberger and Somogyi, 2008). Also, our model addressed two important issues: (1) what are the roles of the different experimentally reported classes of hippocampal and septal inhibitory interneurons (Borhegyi et al., 2004; Klausberger and Somogyi, 2008) in the correct ordering of spatial memories in CA1, and
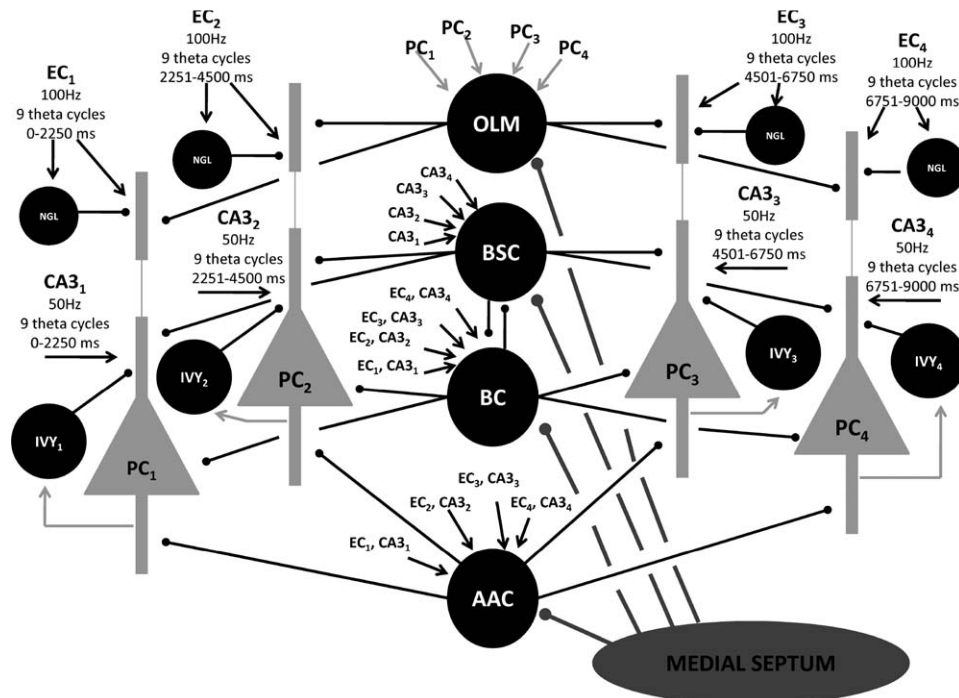
FIGURE 1. Hippocampal CA1 microcircuit showing major cell types and their connectivity. Black arrow lines: excitatory input connections. Black filled circles: CA1 inhibitory connections. Light gray arrow lines: PC excitatory connections. Dark gray filled circles: septal inhibitory connections. EC: Layer III entothinal cortical input. CA3: CA3 Schaffer collateral input. PC: pyramidal cell. AAC: axo-axonic cell. BC: basket cell. BSC: bistratified cell. OLM: oriens lacunosum-moleculare cell. NGL: neurogliaform cell. IVY: ivy cell.

(2) how the hippocampal and septal inhibitory interneurons contribute to the generation and maintenance of theta phase precession of pyramidal cells (place cells) in CA1. Preliminary results of this work have been published in Cutsuridis and Hasselmo (2010) and Cutsuridis et al. (2011).

METHODS

Out of a wide range of possible models of region CA1 with different cell types, cell numbers, connectivities, and possible spike inputs timings and although experimental evidence has shown that the relative percentages of pyramidal cells to inhibitory interneurons are 90% to 10% (Baude et al., 2007; Cutsuridis et al., 2010b), we, instead, modeled the present minimal canonical CA1 microcircuit (see Fig. 1), whose properties are detailed in the subsequent subsections, consisting of only four PCs and six types of inhibitory interneurons: a BC, an AAC, a BSC, four IVYs, four NGLs, and an OLM cell, in order to investigate the biophysical mechanisms by which pyramidal cells in CA1 (1) gate, encode, and retrieve spatial memories in the correct order in the presence of various forms of intra- and extrahippocampal inhibition, (2) time their activities with respect to other CA1 and septal interneurons during theta oscillations, and (3) manage to systematically shift their phase of firing to earlier phases of the theta rhythm as the animal transverses the place field (theta phase precession) as it has

experimentally been observed in animals transversing a linear track (O'Keefe and Recce, 1993; Skaggs et al., 1996).

In the model, IVYs, although never reported to be as numerous as PCs, are local interneurons in stratum radiatum (SR) recurrently excited by the PCs (Fuentealba et al., 2008a,b). Similarly, NGLs, although never reported to be as numerous as PCs, are local interneurons in lacunosum-moleculare (LM) layer modulating the perforant path input to each PC's distal dendrites (Fuentealba et al., 2010). Hence, we considered four IVYs and four NGLs in our network, each as the SR and LM inhibitory companion of each PC.

Hodgkin-Huxley mathematical formalism was used to describe the ionic and synaptic mechanisms of all cells (see Appendix). The biophysical properties of each cell were adapted from cell types reported in the literature (White et al., 1998; Dickson et al., 2000; Fransen et al., 2002, 2004; Kunec et al., 2005; Cutsuridis and Wennekers, 2009; Cutsuridis and Hasselmo, 2010; Cutsuridis et al., 2008, 2010, 2011).

Pyramidal Cells

Each CA1 PC consisted of four compartments: an axon, a soma, a proximal dendrite, and a distal dendrite. Active properties included a fast Na^+ current, a delayed K^+ rectifier current, a low-voltage-activated (LVA) L-type Ca^{2+} current, an A-type K^+ current, an h-current and a calcium-activated mAHP K^+ current (see the Appendix for mathematical details of these currents). The conductance of the h-current was set to 0.005
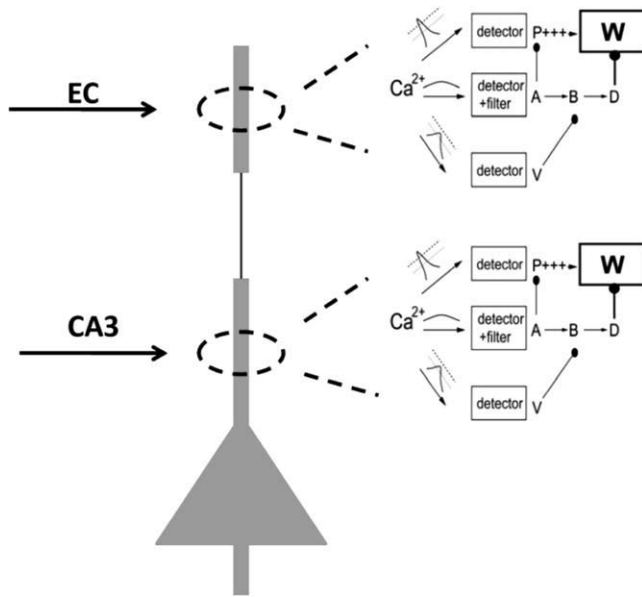
FIGURE 2.   Pyramidal cell model with calcium detectors in distal and proximal dendrites. Synaptic plasticity at the dendritic synapses (circled regions) is governed by two model calcium detector systems. P: potentiation detector; A, B: intermediate elements; D: depression detector activated by B and vetoed by V; V: veto detector; W: synaptic weight. P and D compete to influence the plasticity variable W, which serves as a measure of the sign and magnitude of synaptic strength changes from the baseline.

mS/cm^2 at the soma, 0.01 mS/cm^2 at the proximal dendrite, and 0.02 mS/cm^2 at the distal dendrite. No recurrent connections were assumed between PCs in the network.

Each CA1 PC received AMPA and NMDA excitation from the CA3 Schaffer collaterals and entorhinal cortex (EC) in their proximal and distal dendrites, respectively, and GABA$_A$ synaptic inhibition from BC cells to the soma, from AAC cells to the axon, from BSC and IVY cells to the proximal dendrite and from NGL and OLM cells to the distal dendrite.

Inhibitory Interneurons

All inhibitory interneurons (INs) consisted of a single compartment (soma). Active properties of BC, AAC, BSC, and IVY included a fast Na$^+$, a delayed rectifier K$^+$, a leakage, and a type-A K$^+$ currents (Cutsuridis et al., 2010; Cutsuridis and Hasselmo, 2010). Active properties of the OLM cell included a fast Na$^+$ current, a delayed rectifier K$^+$ current, a persistent Na$^+$ current, a leakage current, and an h-current (White et al., 1998; Dickson et al., 2000; Fransen et al., 2002, 2004; Kunec et al., 2005; Cutsuridis and Hasselmo, 2010), whereas those of the NGL cell included a fast Na$^+$ current, a delayed rectifier K$^+$ current and a leakage current (see the Appendix for mathematical details of these currents).

AAC and BC received excitatory inputs from the EC perforant path and the CA3 Schaffer collaterals and inhibition from the medial septum (MS). AAC was modeled as a burst cell turning on and off before the BC, as it was depicted by the Klausberger and Somogyi (2008) study, where the firing rate

response of AAC ends before the firing rate response of BC [see Fig. 2 in Klausberger and Somogyi's study (2008)]. BC was modeled as a slow integrator [see Fig. 2 in Klausberger and Somogyi's study (2008)]. The BC received additional inhibition from the BSC. The BSC was excited by the CA3 Schaffer collateral input only, inhibited by the MS and the BC. Each IVY cell in the network was recurrently excited by its companion PC. NGL cells were excited by the EC input only and inhibited by the OLM cell (Capogna, 2011). The OLM cell received recurrent excitation from all PCs and feedforward inhibition from the MS.

Model Inputs

The dynamics of the network were influenced by a number of external inputs. Excitatory inputs (spikes) to network cells originated from the EC and the CA3 Schaffer collaterals, whereas external GABA$_A$ inhibitory input originated from the MS. The EC input excited the distal dendrites of the PCs, whereas the CA3 input excited the proximal dendrites.

Each pyramidal cell in the network received a different set of EC and CA3 inputs (PC$_1$ was excited by EC$_1$ and CA3$_1$, PC$_2$ by EC$_2$ and CA3$_2$, PC$_3$ by EC$_3$ and CA3$_3$ and PC$_4$ by EC$_4$ and CA3$_4$) (see Fig. 1). The proper order by which the EC and CA3 inputs were presented to each PC (EC$_1$ and CA3$_1$ first, followed by EC$_2$ and CA3$_2$, then by EC$_3$ and CA3$_3$ and finally by EC$_4$ and CA$_4$) was ensured (gated) by dopamine in the LM layer (see Dopamine Modulation section for details). The duration of each set of EC and CA3 inputs is 2,250 ms [this corresponds to nine theta cycles, each theta cycle with duration of 250 ms; this was designed to match the average number of theta cycles within a place field (Maurer and McNaughton, 2007)]. The presentation frequencies of the EC and CA3 inputs are set to 100 Hz (interspike interval, ISI = 10 ms) and 50 Hz (ISI = 20 ms), respectively (Colgin et al., 2009).

Inhibitory MS inputs (spikes) were turned on and off at specific phases of the theta rhythm. One MS input was turned on near the peak of the extracellular theta (MS$_{180}$) (Borhegyi et al., 2004), whereas the other one near its trough (MS$_{360}$) (Dragoi et al., 1999). All network inhibitory interneurons except for the IVY and NGL cells were inhibited by the MS inputs (Borhegyi et al., 2004).

Presynaptic GABA$_B$ Inhibition

A presynaptic GABA$_B$ inhibition that cyclically changed with respect to the external theta rhythm (Molyneaux and Hasselmo, 2002) modulated the strength of Schaffer collateral input to the PC proximal synapses. This GABA$_B$ modulation was modeled with a 50% reductive scaling of the CA3 input strength during the peak phase of each theta cycle and a lack of reductive scaling of the CA3 input strength during the trough phase (Cutsuridis et al., 2010).

Synaptic Plasticity

A mechanism for STDP in each PC dendrite was used to model plasticity effects. The mechanism had a modular structure consisting of three biochemical detectors: a potentiation (P) detector, a depression (D) detector, and a veto (V) detector

(Rubin et al., 2005). Each detector responded to the instantaneous calcium level and its time course in the dendrite. The potentiation (P) detector triggered LTP every time the calcium levels were above a high-threshold (4 μM). The depression (D) detector detected calcium levels exceeding a low threshold level (0.6 μM). When the calcium levels remained above this threshold for a minimum time period, LTD was triggered. The veto (V) detector detected levels exceeding a midlevel threshold (2 μM) and triggered a veto to the D response. P and D compete to influence the plasticity variable W [see Eq. (30)], which serves as a measure of the sign and magnitude of synaptic strength changes from the baseline.

Calcium entered the neuron through: (1) voltage-gated calcium channels (VGCCs) and (2) NMDA channels located at each dendrite. Plasticity resulted from the synergistic action of these two calcium sources (NMDA and VGCC). A graphical schematic of the model pyramidal cell and its calcium detectors for STDP is shown in Figure 2.

During the peak phases of theta the AMPA and NMDA synaptic conductances in the proximal dendrite of the PCs were modeled as

$$g_{syn} = (w_s \cdot w + W) \cdot g_{max} \qquad (1)$$

where w_s is the scaling factor (set to 0.5 for the present simulations) due to presynaptic GABA$_B$ inhibition, w is synaptic strength, and W is given by Eq. (29). During the trough phases of theta the GABA$_B$ inhibition was removed (i.e. $w_s = 1$) and the proximal AMPA and NMDA conductances were described as,

$$g_{syn} = (w + W) \cdot g_{max} \qquad (2)$$

During theta the AMPA and NMDA synaptic conductances in the distal dendrites of the pyramidal cells were described by

$$g_{syn} = (w + W) \cdot g_{max} \qquad (3)$$

Dopamine Modulation

In the hippocampus the primary targets of DA are the subiculum and region CA1 (Gasbarri et al., 1997). In CA1, the distal and proximal dendrites of pyramidal neurons are both targeted by the DAergic neurons (Cobb and Lawrence, 2010). Previous studies have shown that when DA is applied to the bathing solution, the field-EPSP (fEPSP) evoked by the EC temporoammonic (TA) pathway stimulation is depressed, whereas the fEPSP by the CA3 Schaffer collateral (SC) pathway stimulation remains unaltered (Otmakhova and Lisman, 1999). Subsequent studies by Ito and Schuman (2007) demonstrated that DA acts as a gate on the direct cortical input to the CA1 PC distal dendrites, modulating the information flow and the synaptic plasticity in a frequency-dependent manner. During low frequency stimulation, DA depresses the excitatory TA inputs to both CA1 pyramidal cells and NGL interneurons via presynaptic inhibition, whereas during high frequency stimulation, DA potently facilitates the TA excitatory drive onto CA1
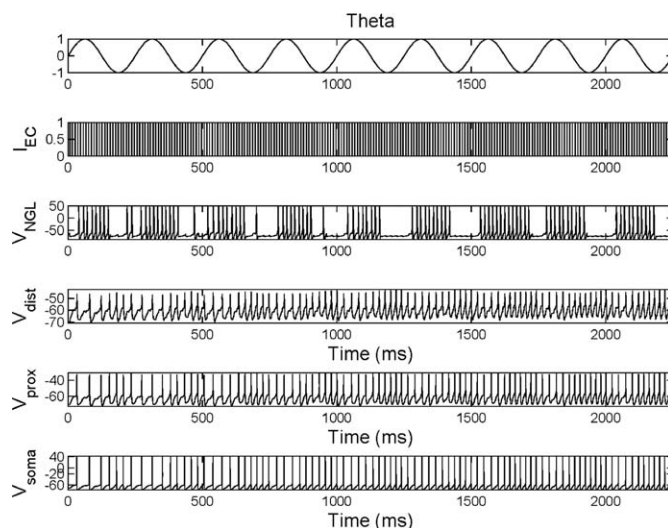
FIGURE 3. (A) Voltage traces of a pyramidal cell (place cell) firing inside its firing field with respect to the external theta oscillation in the presence of high frequency EC (100 Hz) input and NGL inhibition. All other inhibitory cells, although present in this simulation run, do not connect with the pyramidal cell, but only with each other. The NGL cell discharges during the peak phase of theta and remains silent during the trough phase of theta due to the recurrent OLM inhibition, which discharges during the trough phase of theta (see Fig. 7D). In order to simulate the high-pass filter properties of DA during high frequency stimulation (i.e. when the cell is inside its place field), then the strength of the NGL inhibition to PC distal dendrites remained unchanged and the DA level is reduced to 0.73, thus reducing the inhibitory effects of the NGL to PC distal dendrite. Note the presence of high frequency dendritic spikes at the distal PC dendrites even in the presence of high frequency NGL inhibition. These distal PC dendritic spikes propagate to the PC soma and generate action potentials. The PC discharge frequency increases in every subsequent theta cycle due to the continuously increasing synaptic weight in the proximal and distal PC dendrites due to STDP (data not shown).

pyramidal neurons, while diminishing the feedforward NGL inhibition to the distal PC dendrites.

Although we did not explicitly model the activity of DA cells, we assumed a tonic presence of DA and modeled effects of the tonic DA in the following way [see Eq. (50)]: when a pyramidal cell (place cell) was inside its place field, then high frequency EC stimulation impinged on both NGL interneuron and the PC distal dendrite. During this high frequency stimulation environment, the strength of the NGL inhibition to PC distal dendrites was set to 1.1 ($w_{ngl-to-pc} = 1.1$), whereas the DA level was set to 0.73, thus reducing the inhibitory effect of the NGL cell to the PC distal dendrite and hence opening the gate. Dendritic spikes in the distal PC dendtites are evident, which propagate to the PC soma and generate action potentials (see Fig. 3). On the other hand, when a place cell was outside its place field, then both PC and NGL neurons received low frequency EC and CA3 stimulations [one to three spikes per theta cycle (Alonso and Garcia-Austt, 1987)]. Although the strength of the NGL inhibition to PC distal dendrites remained unchanged, the modulation level of DA on the strength of the NGL inhibition was increased to 1 in order to
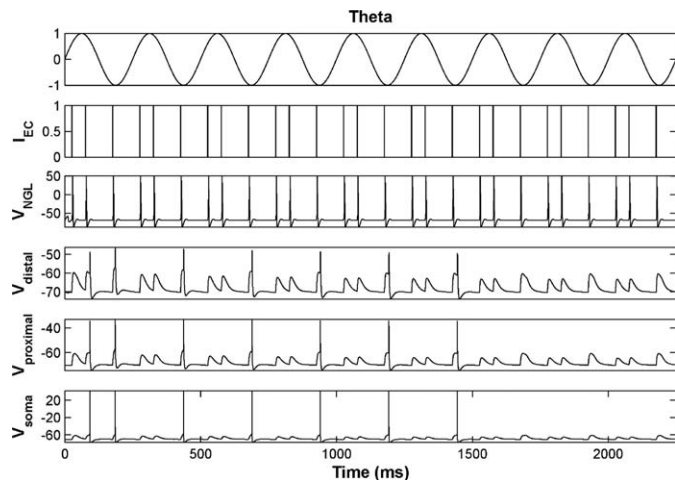
FIGURE 4.   Voltage traces of a pyramidal cell (place cell) firing outside its firing field in the presence of low frequency EC input, DA modulation, and NGL inhibition. All other inhibitory cells, although present in this simulation run, do not connect with the pyramidal cell, but only with each other. The strength of the NGL inhibition to PC distal dendrites ($w_{NGL-to-PC}$) is set to 1.1 and the DA level to 1, in order to simulate the closing of the gate by DA (see Dopamine Modulation section for details). Note the pyramidal cell fires at low frequency (at most one spike per theta cycle) due to the increased feedforward NGL inhibition.

simulate the closing of the gate by DA. The low-frequency stimulation then allowed the NGL to feedforwardly inhibit the PC distal dendrites, thus causing the PC to stop firing or at most fire one spike per theta cycle (see Fig. 4).

RESULTS

Gating and Timing of Spatial Memories During Theta Oscillations

Successful spatial navigation requires the encoding (storage) and retrieval (remembering) of spatial locations in the hippocampus in a sequential manner across time. In this article, encoding refers to the modification of synapses of place cells responding to sequentially visited locations. Retrieval refers to the sequential reactivation of the next place cell by activity in the place cell that preceded it during encoding. Successful retrieval of spatial memories in time requires encoding these memories in the correct order. Such an ordering of memories may be accomplished by the opening of gates (gating) in the correct order. Gating refers to the regulation of inhibitory influences to allow the appropriate neural activity during specific functional phases. Below we describe the mechanisms by which gating, encoding, and retrieval of spatial memories may occur in region CA1 of the hippocampus.

The virtual paradigm we simulated was a rat running on a linear track (see Fig. 5). In our environment the rat had to visit four places ("place 1," "place 2," "place 3," and "place 4") in order to traverse the track. Each place was encoded by a differ-

ent pyramidal cell (place cell) in the CA1 network ("place 1" by PC_1, "place 2" by PC_2, "place 3" by PC_3 and "place 4" by PC_4), which fired at high frequency when the cell was inside its place field (see Fig. 3) and at low frequency (or did not fire) when the cell was outside the PF (see Fig. 4). The time the rat spent inside a PF was equal to the duration of nine theta cycles, with each theta cycle lasting 250 ms, a total duration of 2,250 ms. This was used to model the average duration of running time through an individual place field (Maurer and McNaughton, 2007). At time $t = 0$ ms and when the PC_1 (place cell) was inside its place field (0–2,250 ms), a high frequency (100 Hz) input from EC_1 excited both the NGL_1 interneuron and the distal PC_1 dendrite.

During this high frequency input for the PC_1, the selective effects of DA modulation on high frequency input opened the gate to encoding and retrieval by PC_1 of the place 1 memory pattern (EC_1) and its context ($CA3_1$) during the theta oscillation. DA opened this gate by setting the strength of the NGL_1 inhibition to PC_1 distal dendrite to a low value, thus reducing the NGL inhibition to the PC distal dendrites and facilitating the EC_1 excitatory drive onto PC distal dendrites (Ito and Schumann, 2007). At the same time DA closed the gate to encoding and retrieval by PC_{2-4} of place 2–4 memory patterns (EC_{2-4}) and their contexts ($CA3_{2-4}$). DA closed these gates by setting the strength of the NGL_{2-4} inhibition to PC_{2-4} distal dendrites to a high value, thus increasing the NGL inhibition to the PC distal dendrites and suppressing the effect of the EC_{2-4} excitatory drive onto the PC_{2-4} distal dendrites. Concurrently with the high frequency EC_1 input to PC_1, a low frequency (50 Hz) input from CA3 Schaffer collaterals ($CA3_1$) excited the proximal dendrites of the PC_1. On its own, the EC_1 input generated dendritic spikes, which propagated to the soma and generated action potentials in the PC_1 soma (see Fig. 6A) (Brun et al., 2002, 2008). Similarly, the $CA3_1$ input generated excitatory postsynaptic potentials (EPSPs), which failed to generate somatic action potentials in PC_1 during the first half of the theta rhythm, because its strength to PC_1 proximal dendrites was reduced by 50% due to presynaptic $GABA_B$ inhibition (see Presynaptic $GABA_B$ Inhibition section for details) (see Fig. 6B) (Brun et al., 2002, 2008). When the EC_1 and $CA3_1$
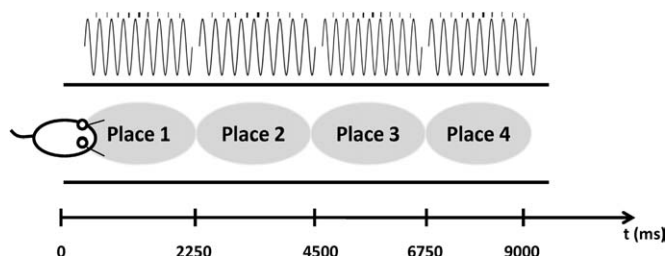
FIGURE 5.   A rat running along a linear track. Gray filled ellipses represent the place fields of four pyramidal cells (place cells) in the network. Note their fields are nonoverlapping. The time the rat spends in each place field is equal to nine theta cycles, with each theta cycle lasting 250 ms, a total time of 2,250 ms. As the rat transverses the place field, each PC shifts its firing to earlier phases of the theta rhythm.
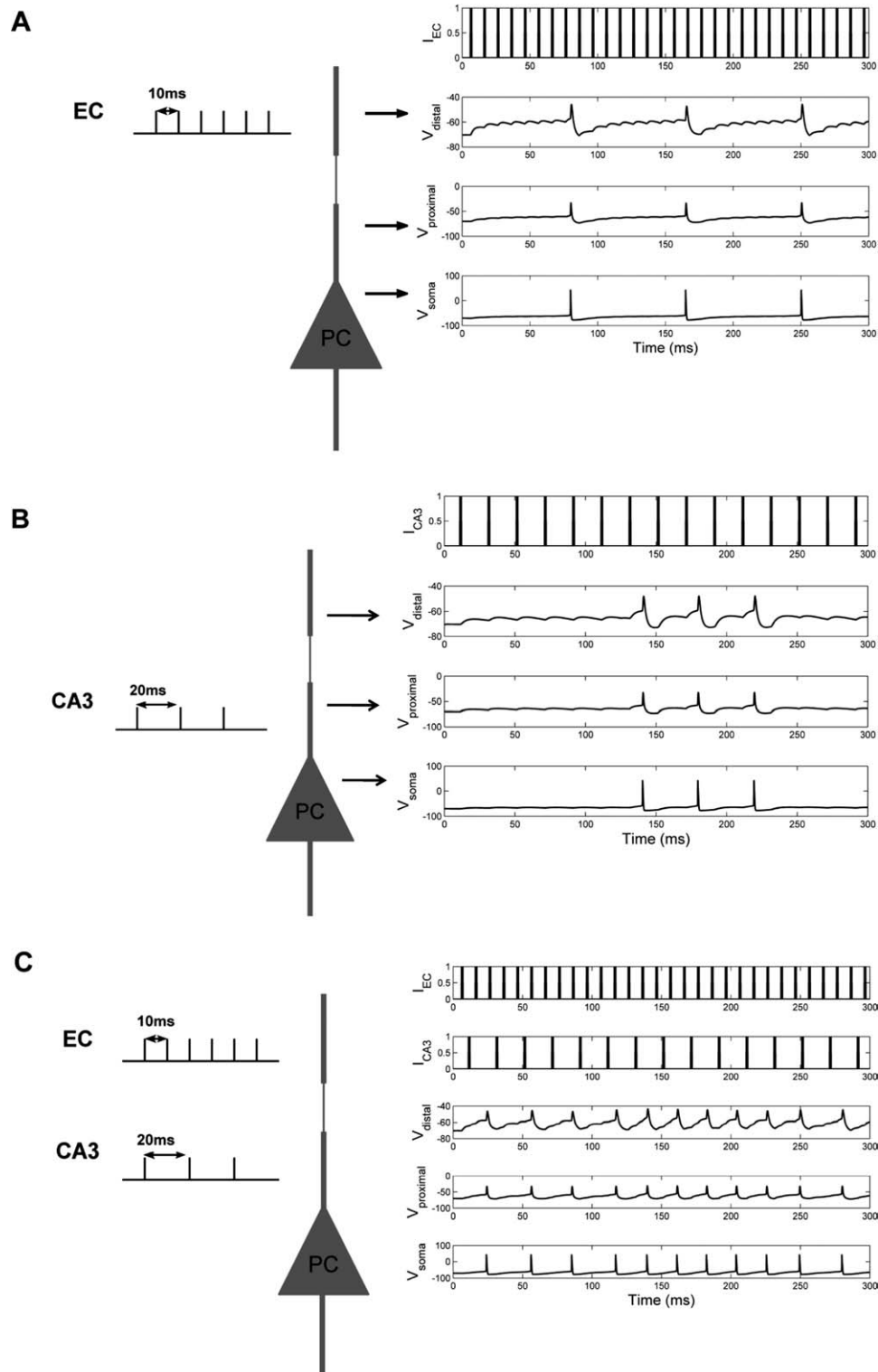
FIGURE 6. (A) Response of the soma, proximal dendrite, and distal dendrite of the model pyramidal cell when only the EC input impinges on its distal dendrite. All inhibition is switched off in this example. When the presentation frequency of the input is high (100 Hz) it produces dendritic spikes, which propagate toward the soma and generate action potentials (Burn et al., 2002, 2008). (B) Response of the soma, proximal dendrite, and distal dendrite of the model pyramidal cell when only the CA3 Schaffer collateral input impinges on its proximal dendrite. All inhibition is switched off in this example. Note that when the presentation frequency of the input is high (50 Hz), it produces dendritic spikes only during the second half of theta when presynaptic GABA$_B$ inhibition is lifted off (Brun et al., 2002, 2008) (see Model Architecture and Properties section for details). (C) Response of the soma, proximal dendrite, and distal dendrite of the model pyramidal cell when both the EC and the CA3 Schaffer collateral inputs impinge on the distal and proximal dendrites of the pyramidal cell. All inhibition is switched off in this example.
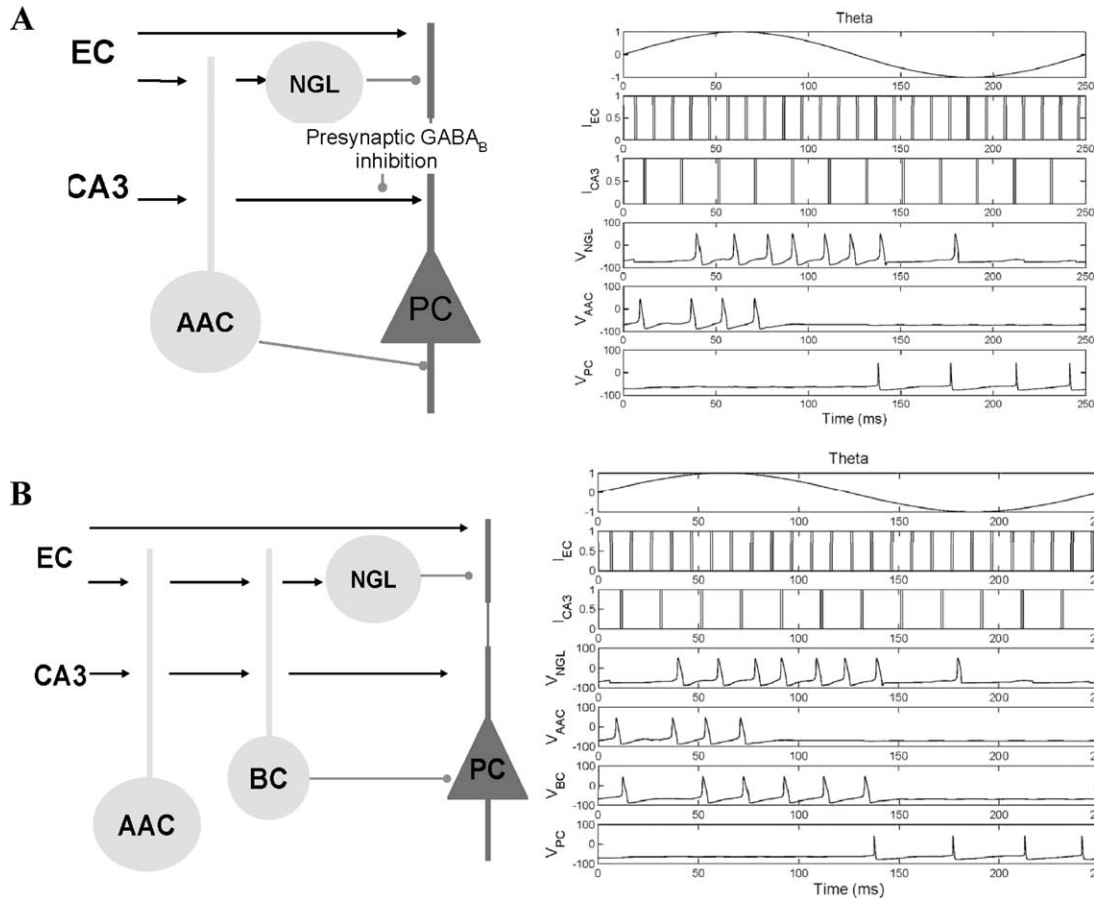
FIGURE 7.   Schematic of how model cells operate and their corresponding firing responses during a theta cycle (0–250 ms). (A) Continuously and concurrently present during the entire theta cycle gamma modulated EC (100 Hz) and CA3 (50 Hz) inputs excite the AAC, which in turn inhibit the axon of a PC, thus pausing the firing of the PC for the most part of the peak phase of theta (0–100 ms). At the same time the EC input excites the PC distal dendrite and the NGL cell, which in turn inhibits the distal dendrites of the PC. The strength of the CA3 input to the proximal dendrite is suppressed by 50% during the peak phase of theta by the presynaptic $GABA_B$ inhibition. This inhibition is removed during the trough phase of theta. (B) When the AAC stops firing, the BC which is excited by the EC and CA3 inputs starts firing, which inhibits the PC soma and prevents the PC from firing for the remaining of the peak phase of theta. (C) BC inhibits during the peak phase of theta with the help of the MS_{180} the BSC, thus preventing it from interfering with the forward association of the EC and CA3 inputs at the proximal PC dendrite. MS_{180} also inhibit the OLM, which in turn dis-inhibit the PC distal dendrite as well as the MS_{360}, which dis-inhibits the AAC and BC. (D) During the trough phase of theta the presynaptic $GABA_B$ inhibition to the CA3 input to the PC proximal dendrite is removed and the MS_{360} is turned on. BC, AAC, and MS_{180} are now inhibited by the MS_{360} inhibition, thus releasing the PC, BSC, and OLM cells from inhibition. In turn OLMs inhibit the NGLs. Recurrent excitation from the PC excites the IVY cells.

inputs arrived at the same time at the proximal dendrites of the PC_1, then action potentials were generated in the PC_1 soma (see Fig. 6C) (Jarsky et al., 2005).

However, as experimental evidence (Klausberger et al., 2003, 2004; Klausberger and Somogyi, 2008) has shown, the PCs are silent during the peak phase of theta [90–270° in the Klausberger studies (2003, 2008)]. In the model presented here, the peak phase of theta corresponds to an encoding phase when input modifies the strength of synapses but does not evoke spiking output at the soma. During the peak phases of theta, the coincident EC_1 and $CA3_1$ inputs caused first the AAC to fire action potentials (APs), which inhibited the axons of PC_1 and prevented it from firing APs (Klausberger et al., 2003) (see Fig. 7A). Once the AAC stopped firing, then the BC, which was modeled as a slow integrator (Klausberger

et al., 2003), started firing due to the coincident EC_1 and $CA3_1$ inputs to its soma (see Fig. 7B). The role of the BC was to inhibit the PC_1 and prevent it from firing as well as to contribute with the septal MS_{180} input to the inhibition of the BSC (see Fig. 7C), whose inhibition could affect the forward association of the EC_1 and $CA3_1$ inputs in the PC_1 proximal dendrite by reducing the rate of change of the synaptic weight there (data not shown). The BSC, along with the OLM cell, were inhibited by the septal MS_{180} inhibitory input, which was turned on during the peak phase of the theta oscillation (see Fig. 7C). The septal MS_{360} input was off during the peak phase of theta, which in turn disinhibited the AAC and BC, and allowed them to fire and carry-on with their inhibitory functions during the peak phase of theta (see Fig. 7C).
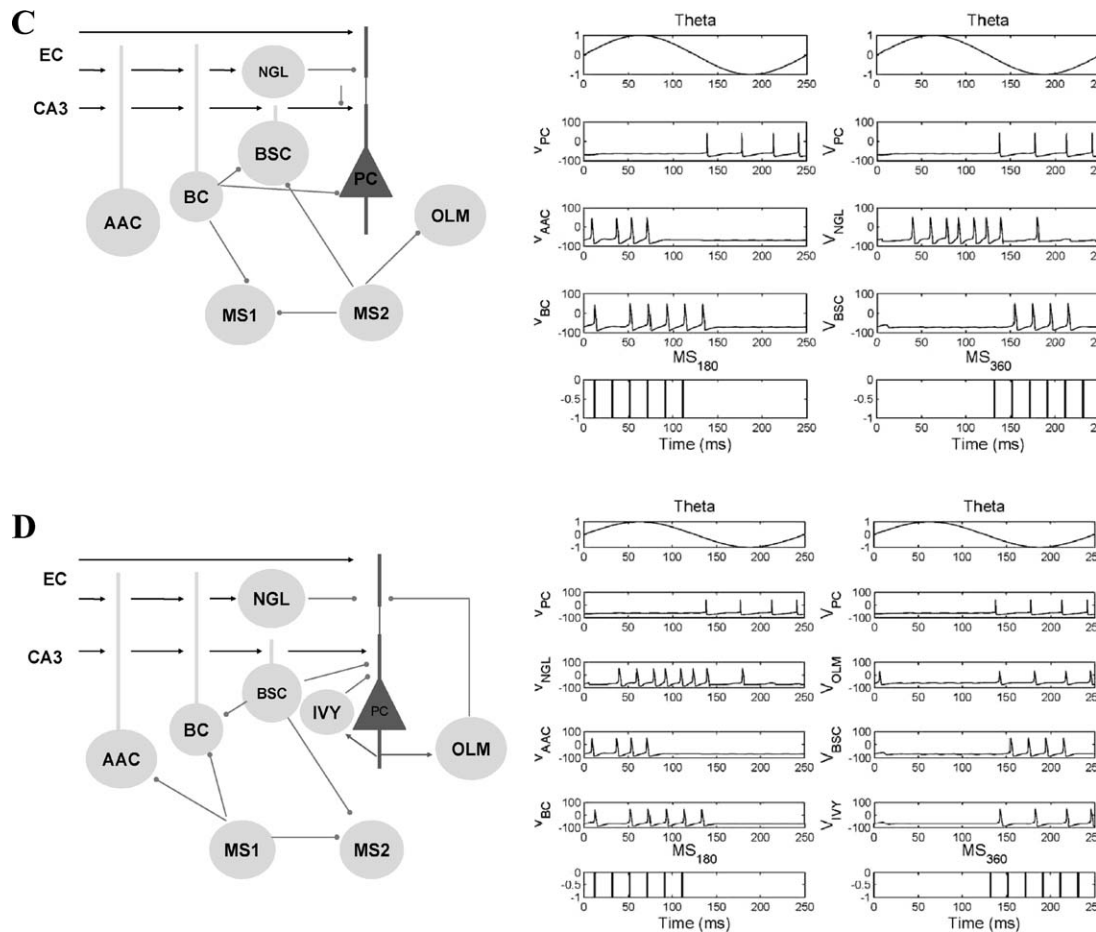
FIGURE 7.   Continued

In contrast to encoding at the peak phase of theta, the trough phase of theta provides dynamics appropriate for retrieval of previously encoded associations. The trough phase of the theta [270–450° in the Klausberger studies (2003, 2004, 2008)] began as the presynaptic $GABA_B$ inhibition to $CA3_1$ Schaffer collateral input to PC_1 synapse was removed and MS_{360} inhibition was turned on (see Fig. 7D). Because of this septal input, the BC and AAC are now inhibited, releasing the PC_1, BSC, and OLM from inhibition (see Fig. 7D). The MS_{180} is now off, which in turn dis-inhibits the BSC and OLM cells (see Fig. 7D). To ensure the "correct" PC fires and hence the "correct" place memory is retrieved, the disinhibited BSC broadcasts to all PCs a nonspecific inhibitory signal, which allows the "correct" PC (in this case the PC_1) driven by the CA3 input in its proximal dendrite to discharge with the proper rate and phase with respect to the theta oscillation [due to the potentiation (via STDP) of the proximal synapse during the peak phase of each theta cycle], while quenching all other PC firing in the network (e.g. subsequent memories in the sequence). The "proper" temporal window with respect to the theta oscillation to which the PC_1 should fire was ensured by the activated IVY cell, which got activated by the recurrent PC_1 excitation and in turn broadcast a second inhibitory signal to the proximal PC_1 dendrite (see Fig. 7D). The OLM cell,

which got activated by all PCs in the network, in turn inhibited the NGLs (Capogna, 2011) and the distal PCs' dendrites allowing the CA3 input to drive the PC(s) during retrieval. As we shall see in the next section, the CA3 input drove CA1 PCs and INs to show theta phase precession.

During every theta cycle, the distal and proximal dendrites of each PC were potentiated or depressed according to a local STDP rule applied to each dendrite, which measured whether the peak and time course of each calcium spike was above a certain threshold (4 μM for potentiation, 2 μM for veto, and 0.6 μM for depression) (see Synaptic Plasticity and Appendix sections for details). Figure 8B depicts the time courses of the proximal and distal synaptic strengths during the duration of the all theta cycles the place cell (PC_1) was inside the PF.

At the same time PC_1 was inside its PF (0–2,250 ms) and the encoding and retrieval processes were taking place as described above, PC_{2-4} were outside their PFs. Low frequency EC_{2-4} and $CA3_{2-4}$ inputs impinged on PC_{2-4} distal and proximal dendrites, respectively, causing them to fire one to three spikes per theta cycle due to the frequency dependent role of dopamine (see Dopamine Modulation section for details; see Fig. 4). AAC, BC, BSC, OLM, IVY_{2-4}, and NGL_{2-4} inhibition operated the same way as in the case of PC_1.
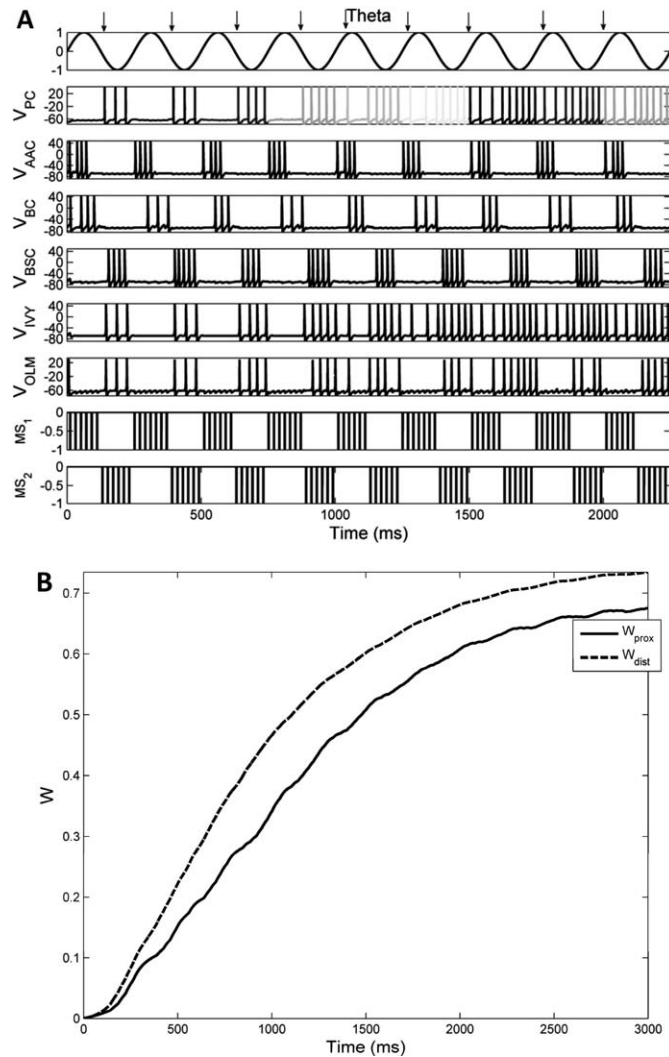
FIGURE 8.   (A) Tonic EC and CA3 inputs to both CA1 pyramidal cells and inhibitory interneurons. Spiking activity of CA1 and septal cells with respect to simulated theta oscillation as measured from the pyramidal layer of CA1. Arrows indicate the phase the place cell fired with respect to theta. Note that at the beginning of the PF (first theta cycle), the place cell fired near the trough of theta. As the rat approached the end of the PF (ninth theta cycle), the place cell fired just after the peak of theta, having precessed almost by 180°. (B) Synaptic strengths of CA1-PC proximal and distal dendrites as a function of time.

Similar patterns of firing with the respect to the external theta appeared in the remaining three PCs (PC$_2$, PC$_3$, and PC$_4$) in the network when the simulated rat was inside their place fields (not shown). PC$_2$ was activated right after PC$_1$ (2,251–4,500 ms), PC$_3$ right after PC$_2$ (4,501–6,750 ms), and PC$_4$ right after PC$_3$ (6,751–9,000 ms) (see Fig. 1). The correct gating of spatial memories was guaranteed by dopamine which opened the gate to the appropriate memory to be encoded and retrieved by the firing of the proper PC and closed the gate to the inappropriate one(s) on a frequency dependent manner (Ito and Schumann, 2007).

Overall, the dynamics of the model is complex, but different cell types play different functional roles at different phases of

theta rhythm to prevent new information from being retrieved as if it were previously encoded. In summary, during the peak phase of theta (encoding) when new entorhinal input is being encoded, the activity of the AAC and BC cells prevented this activity from being interpreted as retrieval by inhibiting the spiking output from CA1 pyramidal cells. During the trough phase of theta (retrieval), the AAC and BC cells are inhibited by the MS$_{360}$ cells, thus disinhibiting the PCs allowing them to fire (i.e. retrieve the pattern) and excite the OLM cells. The OLM cells serve to inhibit the entorhinal input with new information. The BSC cells provided a general level of inhibition within the network to allow selective firing of the correct pattern for retrieval. The IVY cells, which were recurrently excited by the PC cells, provided a second level of inhibition, which ensured that the PCs fired at the experimentally observed theta phase. The MS input and interactions between interneurons serve to maintain these phase relationships.

In the next section, we investigate the mechanisms of generation and maintenance of theta phase precession of place cells in region CA1.

Mechanisms of Theta Phase Precession in CA1

In addition to place cells firing at the trough phase of theta, place cells have been shown to progressively shift to earlier phases of the theta rhythm as the animal transverses its place field (a phenomenon known as theta phase precession) (O'Keefe and Recce, 1993). The observed properties of the theta phase precession of place cells include the following: (1) all place cells start firing at the same initial phase (O'Keefe and Recce, 1993); (2) the initial phase is on average the same on each entry of the rat into the place field of a place cell; (3) the total amount of phase precession is always less than 360° (O'Keefe and Recce, 1993); (4) the firing rate of the place cell increases as the position of the rat in the place field increases, reaching a maximal value at about 200° and beyond this point it decreases again (Harris et al., 2002; Mehta et al., 2002).

Over the years many computational network and cellular models of phase precession have been proposed (O'Keefe and Recce, 1993; Jensen and Lisman, 1996; Tsodyks et al., 1996; Wallenstein and Hasselmo, 1997; Kamondi et al., 1998; Magee, 2001; Harris et al., 2002; Lengyel et al., 2003; Hasselmo and Eichenbaum, 2005; O'Keefe and Burgess, 2005; Gasparini and Magee, 2006; Thurley et al., 2008; Harvey et al., 2009; Cutsuridis et al., 2011). These models make different predictions about the mechanisms giving rise to the theta phase precession, which depend on their initial assumptions regarding the nature of the inputs. For example, in the dual oscillator interference model (O'Keefe and Burgess, 2005), two sets of theta-modulated inputs at different frequencies interfere to create a beat-like pattern of membrane potential fluctuations. In other models (Tsodyks et al., 1996), symmetric or asymmetric ramp inputs interact with the theta-modulated inhibitory inputs.

Here we investigate how the interaction of the EC and CA3 inputs presented at different frequencies and phases with
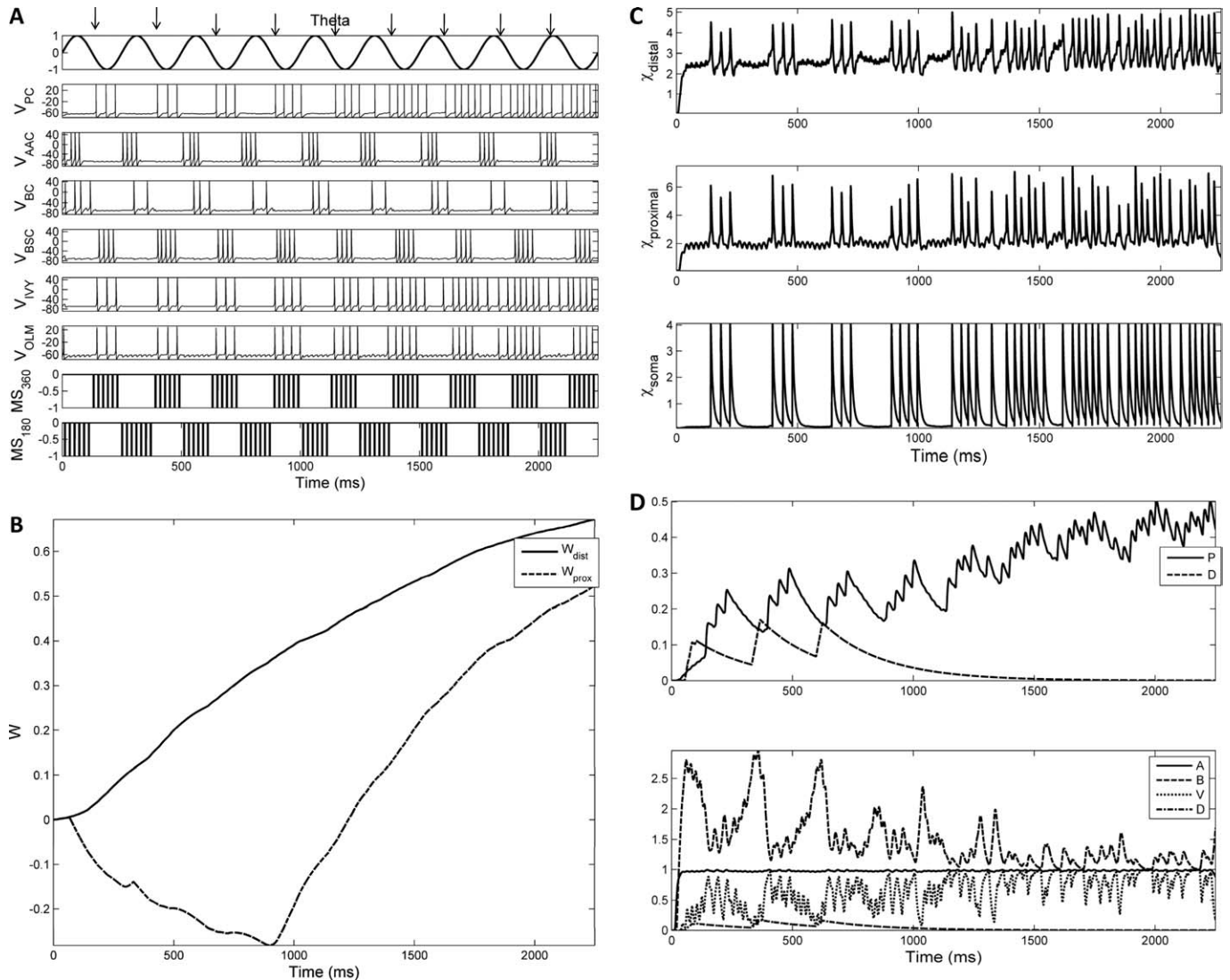
FIGURE 9. **(A) Tonic EC and CA3 inputs to CA1 inhibitory interneurons, tonic EC input to pyramidal cells, and constant frequency phase precessing CA3 input to PCs. CA1 interneuron inhibition was set to a low level. Spiking activity of CA1 and septal cells with respect to simulated theta oscillation as measured from the pyramidal layer of CA1. Arrows indicate the phase the place cell fired with respect to theta. Note that due to low and nonprecessed inhibition the place cell fires the same way as in Figure 8. (B) Synaptic strengths of CA1-PC proximal and distal dendrites as a function of time. (C) Time course of calcium (χ) in the soma, proximal, and distal dendrites of the place cell. (D) Time courses of the potentiation (P), depression (D), veto (V), and intermediate elements (A and B) signals. Parameter values used: $w_{\text{ec-to-aac}} = 1.2$, $w_{\text{ca3-to-aac}} = 1.2$, $w_{\text{aac-to-pc}} = 2$, $w_{\text{bc-to-pc}} = 0.7$, $w_{\text{bc-to-bsc}} = 30$, $w_{\text{ivy-to-pc}} = 0.1$. All other synaptic strength parameter values are the same as in Table A1.**

respect to the LFP theta in the presence of different forms of inhibition affect the synaptic plasticity at the distal and proximal dendrites of the PCs and how in turn the interaction of plasticity and inhibition affects the theta phase precession of the network cells. Out of a wide range of possible models, we here focus on four cases: (1) when both pyramidal and inhibitory cells receive tonic input from EC and CA3; (2) when the pyramidal cells receive CA3 input that is phase precessing and tonic input from the EC, whereas the inhibitory interneurons receive tonic input from both EC and CA3 (e.g. through a different population of CA3 cells); (3) when both PCs and INs receive excitatory tonic input from EC, excitatory CA3 phase

precessing input of constant frequency and phase precessing inhibitory input from the septal cells; and (4) when both PCs and INs receive tonic input from EC, CA3 phase precessing input of varying frequency and phase precessing inhibitory inputs from the septum and the activation of presynaptic GABA_B inhibition.

We started our investigation with tonic EC and CA3 inputs present constantly throughout the nine theta cycles of each PF to the excitatory and inhibitory cells in the network. We observe (see Fig. 8A) that at the beginning of the place field (first theta cycle), the PC (place cell) fired its first spike near the trough of the external theta. As the rat approached the end
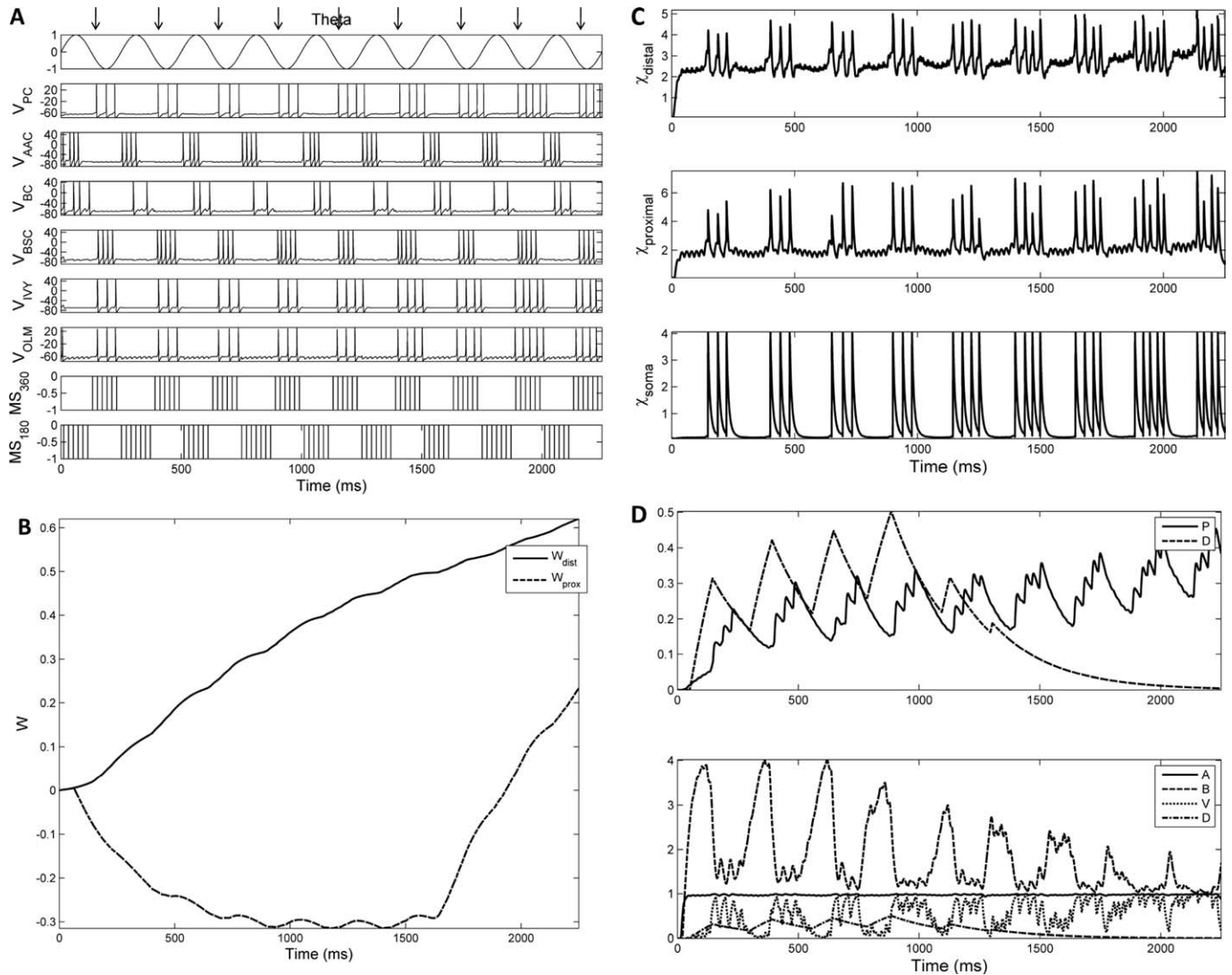
FIGURE 10.   (A) Tonic EC and CA3 inputs to CA1 inhibitory interneurons, tonic EC input to pyramidal cells, and constant frequency phase precessing CA3 input to PCs. Inhibitory interneuron inhibition was set to a high level. Spiking activity of CA1 and septal cells with respect to simulated theta oscillation as measured from the pyramidal layer of CA1. Arrows indicate the phase the place cell fired with respect to theta. Note that due to high and nonprecessed inhibition the place cell fires at the trough of theta in every cycle. **(B)** Synaptic strengths of CA1-PC proximal and distal dendrites as a function of time. **(C)** Time course of calcium (χ) in the soma, proximal, and distal dendrites of the place cell. **(D)** Time courses of the potentiation (P), depression (D), veto (V), and intermediate elements (A and B) signals. Parameter values used: $w_{\text{ec-to-aac}} = 1.2$, $w_{\text{ca3-to-aac}} = 1.2$, $w_{\text{aac-to-pc}} = 2$, $w_{\text{bc-to-bsc}} = 30$, $w_{\text{ivy-to-pc}} = 0.1$, $w_{\text{bc-to-pc}} = 0.7$. All other synaptic strength parameter values are the same as in Table A1.

of the place field (ninth theta cycle), the PC fired just after the peak of theta, having precessed almost 180°. This phase advancement was due to the constantly increasing strength of the proximal PC synapse due to the STDP rule (see Fig. 8B), which increased the tendency of the PC to fire at earlier phases with respect to theta in the presence of a constant level of an inhibitory threshold (BSC inhibition). However, although the PC discharges at earlier phases of theta as the rat transverses the field, it continues to fire at all phases of the theta cycle. Furthermore, its firing rate continuously increases as the rat approaches the end of the field and it remains anchored to the end of the theta cycle. These latter findings come in disagreement with the

experimentally observed evidence (O'Keefe and Recce, 1993; Skaggs et al., 1996; Kamondi et al., 1998; Harris et al., 2002; Mehta et al., 2002), where the entire spike sequence of PC firing precessed and its firing rate increased as the rat approached the middle of the place field, reached its maximum just after the middle of the field and decreased as the rat approached the end of the field. Also, the phase relationships of the INs with respect to the PCs and the LFP theta are disrupted (Klausberger et al., 2003, 2004; Somogyi and Klausberger, 2005; Klausberger and Somogyi, 2008; Klausberger, 2009).

Next we investigated the case where tonic EC and CA3 inputs excited the INs, tonic EC input excited the distal den-
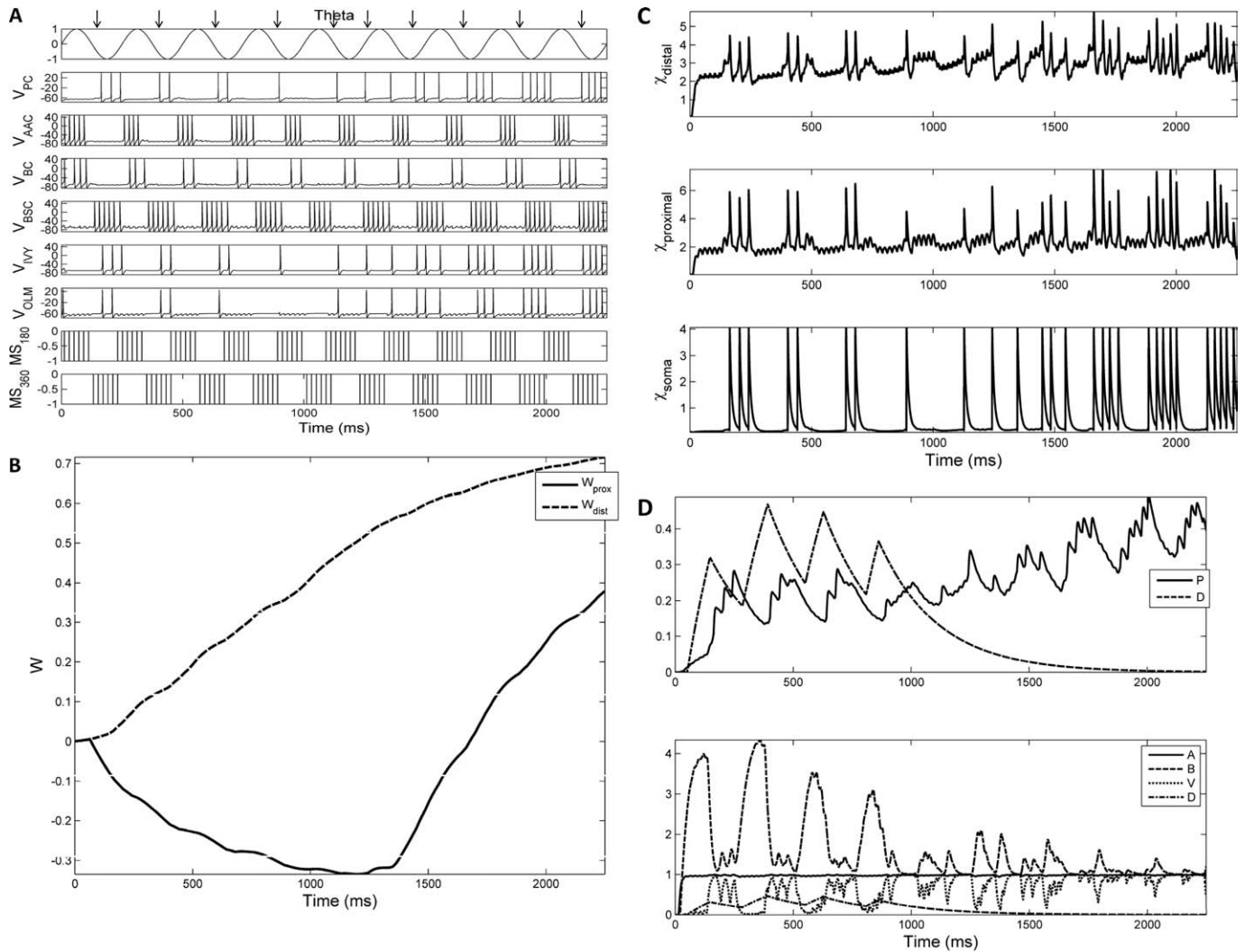
FIGURE 11.   (A) Tonic EC and CA3 inputs to CA1 inhibitory interneurons, tonic EC input to pyramidal cells, constant frequency phase precessing CA3 input to PCs, and phase precessing septal inhibitory input to CA1 inhibitory interneurons. Spiking activity of CA1 and septal cells with respect to simulated theta oscillation as measured from the pyramidal layer of CA1. Arrows indicate the phase the place cell fired with respect to theta. Note that the place cell starts with high firing rate (three spikes in first theta cycle) at the trough of theta and precesses to a full 360° by the ninth theta cycle. However, its firing rate is not consistent with the experimental evidence (Harris et al., 2002; Mehta et al., 2002) since it continues to increase even when the rat approaches the end of the place field (ninth theta cycle). (B) Synaptic strengths of CA1-PC proximal and distal dendrites as a function of time. (C) Time course of calcium (χ) in the soma, proximal, and distal dendrites of the place cell. (D) Time courses of the potentiation (P), depression (D), veto (V), and intermediate elements (A and B) signals. Parameter values used: $w_{\text{ec-to-aac}} = 1.2$, $w_{\text{ca3-to-aac}} = 1.5$, $w_{\text{ca3-to-bc}} = 1$, $w_{\text{aac-to-pc}} = 1.1$, $w_{\text{bc-to-pc}} = 0.6$, $w_{\text{bc-to-bsc}} = 30$, $w_{\text{ca3-to-bsc}} = 1$, $w_{\text{olm-to-pc}} = 0.1$, $w_{\text{pc-to-olm}} = 1.3$, $w_{\text{ivy-to-pc}} = 0.1$, $w_{\text{ngl-to-pc}} = 0.1$. All other synaptic strength parameter values are the same as in Table A1.

drites of the PCs, but phase precessing CA3 input excited the proximal dendrites of the pyramidal cells. The CA3 input was modeled to precess by approximately 40° in every subsequent theta cycle having precessed a full 360° by the ninth theta cycle. When the INs inhibition was low (see Fig. 9A), then PCs fired in a similar way as in the previous case. When the INs inhibition was high (see Fig. 10A), then the discharge pattern of the pyramidal cells did not precess at all. Therefore PC firing is restricted to the trough of the theta oscillation (Klausberger et al., 2003, 2004; Klausberger and Somogyi, 2008). The between-phase relationships of firing of the pyramidal cell

with respect to the various inhibitory interneurons with respect to the external theta are also preserved (Klausberger et al., 2003, 2004; Klausberger and Somogyi, 2008). In both cases (low and high inhibition), the proximal synaptic weight decreased during the first few theta cycles and then it linearly increased till the end of the simulation run. This was due to the nonlinear interaction of the GABA inhibition and the calcium accumulation in the PC proximal dendrite, which depressed it for most of the theta cycles. In the first few theta cycles of each case, GABA inhibition is dominating, thus calcium level is below the 2 µM threshold [i.e. depression (D) de-
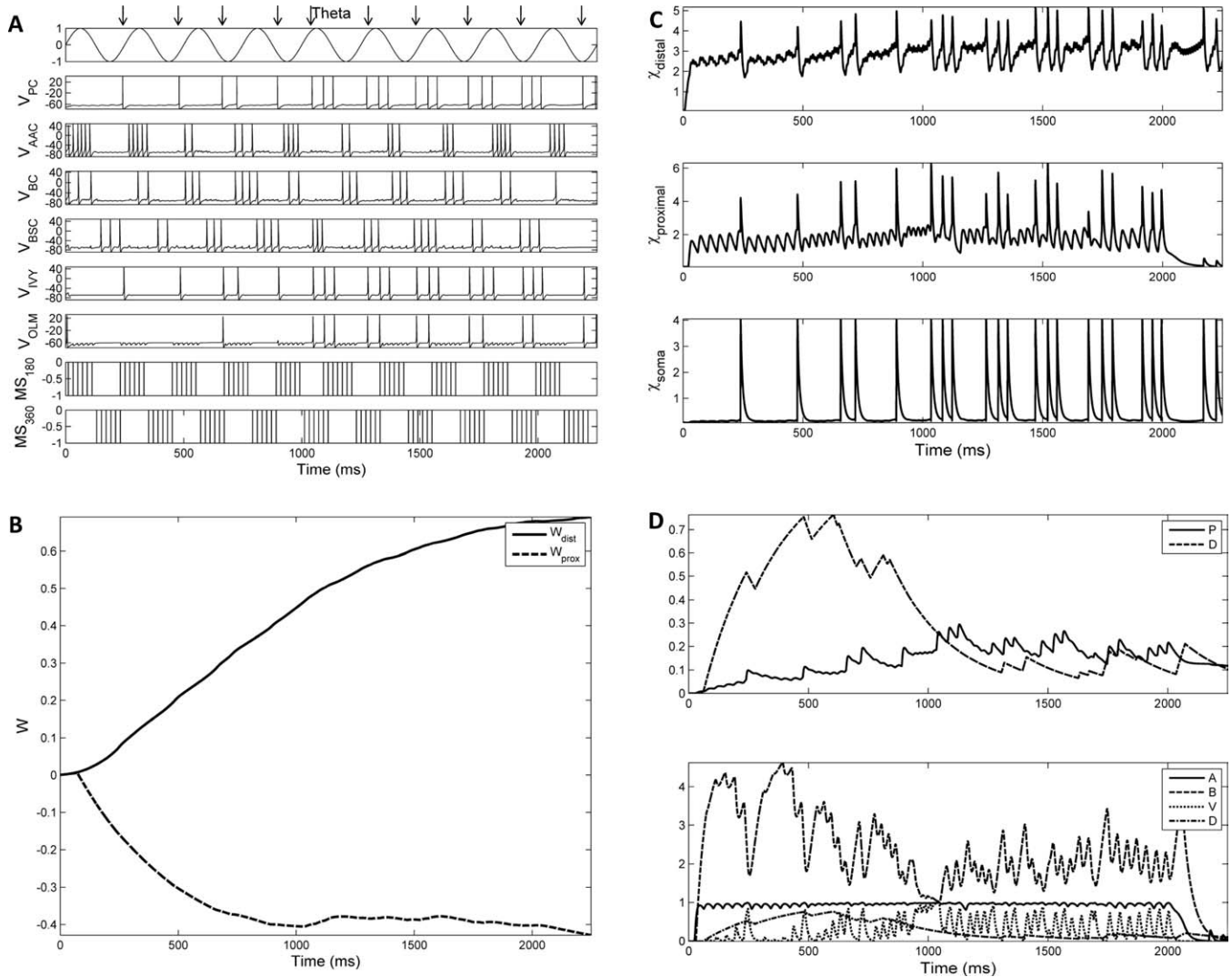
FIGURE 12.   (A) Tonic EC and CA3 inputs to CA1 inhibitory interneurons, tonic EC input to pyramidal cells, varying frequency phase precessing CA3 input to PCs and constant frequency phase precessing septal and presynaptic GABA$_B$ inhibitory inputs to CA1 inhibitory interneurons. Spiking activity of CA1 and septal cells with respect to simulated theta oscillation as measured from the pyramidal layer of CA1. Arrows indicate the phase the place cell fired with respect to theta. Note all experimentally observed characteristics of theta phase precession (see Mechanisms of Theta Phase Precession in CA1 section for details) are captured. (B) Synaptic strengths of CA1-PC proximal and distal dendrites as a function of time. (C) Time course of calcium (χ) in the soma, proximal, and distal dendrites of the place cell. (D) Time courses of the potentiation (P), depression (D), veto (V), and intermediate elements (A and B) signals. Parameter values used: $w_{ec-to-aac} = 1.2$, $w_{ca3-to-aac} = 1.2$, $w_{ca3-to-bc} = 1$, $w_{aac-to-pc} = 1.1$, $w_{bc-to-pc} = 0.6$, $w_{bc-to-bsc} = 30$, $w_{ca3-to-bsc} = 1$, $w_{olm-to-pc} = 0.1$, $w_{pc-to-olm} = 1.3$, $w_{ivy-to-pc} = 0.1$, $w_{ngl-to-pc} = 0.1$. All other synaptic strength parameter values are the same as in Table A1.

tector is turned on] (see Figs. 9C and 10C) and the SC synaptic weight is decreasing (see Figs. 9B and 10B). After the first few theta cycles, the calcium level crosses the 2 μM threshold and the veto (V) signal is turned on, which inhibits the depression (D) signal and allows the potentiation (P) signal to take over (see Figs. 9D and 10D). Thus, the SC synaptic weight starts to monotonically increase (see Figs. 9B and 10B).

Next, we investigated the case where both PCs and INs receive tonic inputs from EC, a CA3 input with constant frequency throughout the place field that is phase precessing and septal inhibition with constant frequency which is also phase precessing by the same amount as the CA3 input. As before

the CA3 input phase advanced by $40°$ in every theta cycle having precessed by a complete $360°$ by the end of the ninth theta cycle (end of the place field). We observe that the PC firing precessed a full $360°$ by the end of the place field and so all INs (see Fig. 11A). The phase relationships between the PCs and INs are also preserved due to the precessing of the septal inhibition. However, the firing rate of the PCs is not consistent with the experimental findings (Harris et al., 2002; Mehta et al., 2002). Their firing rate continues to increase even when the rat approached the end of the field. This was due to the nonlinear interaction of the GABA inhibition and the calcium accumulation in the proximal PC dendrite, which caused the
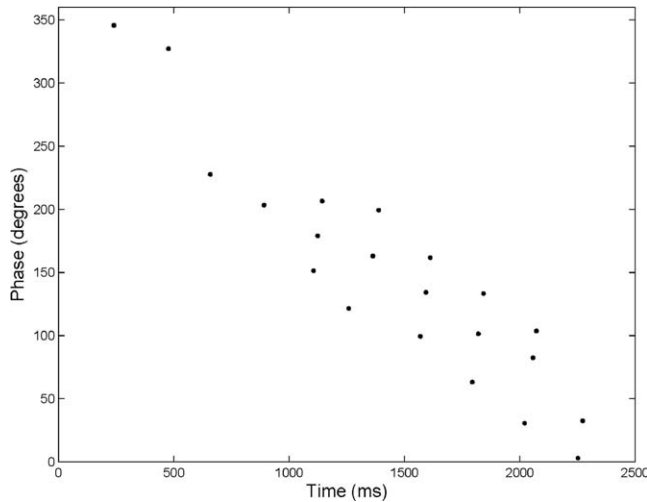
FIGURE 13. Spike phase advancement of a place cell during a linear track running episode. The cell fired sparsely until 1 s into the trial, when an intense period of firing occurred, accompanied by phase precession (Harris et al., 2000).

strength of the proximal PC synapses to increase linearly even toward the end of the place field (see Fig. 11B). As before, in the first few theta cycles, GABA inhibition is dominating, thus calcium level is below the 2 μM threshold [i.e. depression (D) detector is turned on] (see Fig. 11C) and the SC synaptic weight is decreasing (see Fig. 11B). After the first few theta cycles, the calcium level crosses the 2 μM threshold and the veto (V) signal is turned on, which inhibits the depression (D) signal and allows the potentiation (P) signal to take over (see Fig. 11D).

Finally, we investigated the case where both PCs and INs received tonic input from EC, a phase precessed CA3 input whose frequency increased linearly (25–50 Hz) from the start to the middle of the place field and decreased linearly by the same amount from the center to the end of the field. In this case, both septal and presynaptic GABA$_B$ inhibition precessed, but with a constant frequency. We observe (see Figs. 12A and 13) that all of the experimentally observed characteristics of theta phase precession detailed earlier in this section are captured: (1) the firing of the PC starts at the trough of the external theta (beginning of the place field), (2) the firing of the PC phase advances in every subsequent theta, (3) phase precession is almost 360° by the end of the place field (ninth theta cycle), and (4) the firing rate of PC increases as the rat transverses the field, peaks at about 200° and decreases as the rat approaches the end of the place field. The latter is due to the monotonic decrease of the Schaffer collateral synaptic strength throughout the simulation run, thus allowing the phase precessed CA3 input to take charge of the firing of the CA1 PCs (see Fig. 12B). The place cell fired sparsely in the first 1 s of the trial run, after which its firing increased and phase precessed (see Fig. 13). The decrease of the Schaffer collateral synaptic strength was due to the low calcium accumulation level for most of the time (below the 2 μM threshold) in the PC proximal dendrite (see Fig. 12C), which triggered the activation of

the depression (D) signal, which dominated the potentiation (P) in the first four theta cycles and subsequently cancelled each other in the remaining simulation run (see Fig. 12D), thus keeping the synaptic strength depressed (see Fig. 12B). In addition, the firing phase relationships between PCs and INs as they have been observed in the Klausberger studies (2003, 2004, 2008) are preserved. Thus, within these sets of parameters explored here this condition appears to most effectively match the experimental data.

The results of the pyramidal cell firing rate as a function of theta cycle number for the above four cases are summarized in Figure 14.

DISCUSSION

General Issues

The present model is a model of spatial memory sequence encoding and retrieval that simulates accurately many of the experimentally observed biophysical properties of CA1 and MS cells during theta oscillations, suggests functional roles for the dopamine in the gating of information in CA1 in a frequency-dependent manner and for the CA1 pyramidal and inhibitory interneurons as well as medial septal cells in the encoding and
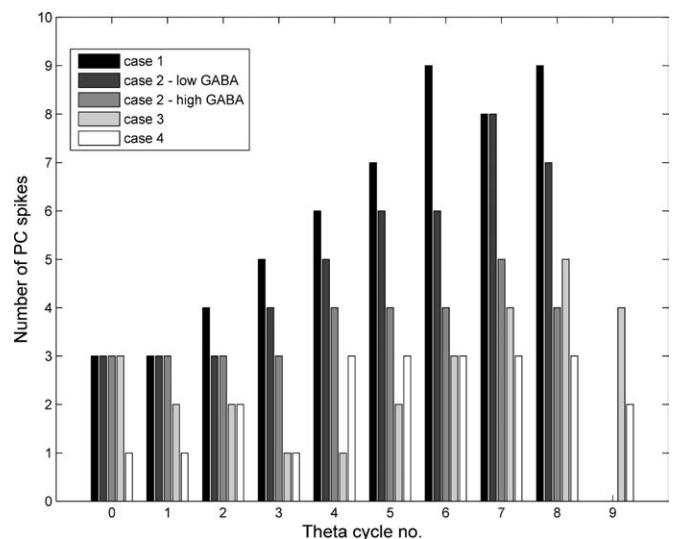
FIGURE 14. Pyramidal cell firing rate as a function of theta cycle number in the four cases identified in the Mechanisms of Theta Phase Precession in CA1 section. *Case 1*: both pyramidal and inhibitory cells receive tonic input from EC and CA3; *Case 2* (low and high GABA): the pyramidal cells receive CA3 input that is phase precessing and tonic input from the EC, whereas the inhibitory interneurons receive tonic input from both EC and CA3 (e.g. through a different population of CA3 cells); *Case 3*: both PCs and INs receive excitatory tonic input from EC, excitatory CA3 phase precessing input of constant frequency, and phase precessing inhibitory input from the septal cells; *Case 4*: both PCs and INs receive tonic input from EC, CA3 phase precessing input of varying frequency, and phase precessing inhibitory inputs from the septum, and the activation of presynaptic GABA$_B$ inhibition.

retrieval of spatial memories in the correct order, and investigates quantitatively the mechanisms for the generation and maintenance of theta phase precession of CA1 pyramidal cells (place cells) in the presence of various forms of intra- and extrahippocampal inhibition. Our model is an extension and revision of the Cutsuridis et al. (2008, 2009, 2010) models of the CA1 microcircuit, which addressed primarily the recall performance and memory capacity of static memory patterns in region CA1. The present model is based on experimentally known intra- and extrahippocampal connectivity (see "Methods" section and References therein for details). Its neural dynamics matched that of the firing activities of dominant cell types in region CA1 and medial septum, such as PCs, AACs, BCs, BSCs, IVY, NGL, OLM, etc. with respect to theta oscillations.

Our model can account for many of the empirical signatures of hippocampal dynamics such as

- CA1 cellular activity coupled to either the peak or the trough of stratum pyramidale theta oscillations with the AAC, BC, and NGL firing at the peak of theta and the OLM, BSC, IVY, and PC firing at the trough of theta (Klausberger et al., 2003, 2004; Somogyi and Klausberger, 2005; Klausberger and Somogyi, 2008; Fuentealba et al, 2008a,b, 2010)
- GABAergic medial septal neuron exhibiting highly regular bursting activity coupled to either the trough or the peak of hippocampal theta rhythm (Borhegyi et al., 2004)
- Dopamine modulating the inflow of EC information (spatial memories) to CA1 PC distal dendrites on a frequency-dependent manner (Ito and Schumann, 2007)
- Pyramidal cell activity in CA1 phase precessing with respect to theta oscillations (O'Keefe and Recce, 1993; Skaggs et al., 1996)
- The initial phase of precession always starting at the end of the theta rhythm and progressively shifted to earlier phases of theta (O'Keefe and Recce, 1993; Skaggs et al., 1996)
- The total amount of phase precession always be less than $360°$ (O'Keefe and Recce, 1993)
- Firing rate of the place cell increasing as the position of the rat in the place field increases, reaching a maximal value at about $200°$ and beyond this point it decreasing again (Harris et al., 2002; Mehta et al., 2002).
- Inhibitory interneuron activity in CA1 phase precessing with respect to theta oscillations (Maurer et al., 2006; Ego-Stengel and Wilson, 2007).
- Inhibitory interneurons showing multiple phase precessing fields with respect to theta (data not shown) (Maurer et al., 2006).

What Have we Learned From the Model?

Gating of cortical information in CA1

The model showed that the ordering of the EC spatial information to CA1 in the correct order is achieved by DA modulation of the strength of the NGL inhibition and EC excitation

onto the PC distal dendrites in a frequency-dependent manner, which acted a gate-keeper (Ito and Schumann, 2007). In particular, during high frequency EC excitation to both NGL cell and PC distal dendrites, the DA levels were kept to a low value, thus diminishing the effects of the NGL inhibition to the PC distal dendrites and allowing distal dendritic spikes due to the impinged high frequency EC excitation to propagate to the soma and generate action potentials (see Fig. 3). Thus, low DA levels opened the gate to the entorhinal-hippocampal dialogue and allowed the memory pattern(s) to be encoded by the CA1 pyramidal cell(s). On the other hand, during low frequency EC excitation to both NGL cell and PC distal dendrites, the DA levels were increased, thus allowing the NGL inhibition to feedforwardly inhibit the PC distal dendrites, causing the PC to stop firing (or at most fire one action potential during a theta cycle), and interrupting the entorhinal-hippocampal dialogue (see Fig. 4).

Timing and roles of cells during theta oscillations

In the presence of continuous EC and CA3 excitation throughout theta the activities of region CA1 inhibitory interneurons were sculpted by MS inhibitory inputs. MS_{180} input inhibited region CA1's BSC and OLM cells during the peak of theta measured in stratum pyramidale, whereas MS_{360} input inhibited the AAC and BC cells during the trough of theta. Because of the MS inhibition the activities of AACs and BCs during the peak phases of theta inhibited the spiking output of PCs, thereby preventing them from firing (i.e. retrieving the memory; see Figs. 7A,B). In contrast, the activity of OLM cells during the trough phase of theta inhibited the NGL cells and the entorhinal input with the new information from interfering with retrieval of the old information (CA3 input to PC proximal dendrites) (see Fig. 7D). The activity of the BSC provided a general inhibitory threshold to all PCs in the network, allowing in this manner the "correct" pyramidal cell to retrieve the pattern (i.e. its tendency to fire has increased due to its sufficient strengthening of its proximal synaptic weight causing it to fire more than three action potentials during the trough phase of theta; see Fig. 7D). The activity of the IVY cell during the trough phase of theta provided a second threshold mechanism which ensured that the pyramidal cell will fire during the experimentally observed theta phase (see Fig. 7D).

Memory function would have been severely impaired if new information arriving in the circuit was interpreted as the retrieval of previously stored information, resulting in false interpretation of new information as old, or in the re-encoding of an old event. Imagine that before you drive home your wife calls to tell you to purchase some milk. If this new encoding is confounded with prior retrieval, you might interpret this new information as if you were remembering an old conversation from the previous week, and therefore think you have already done the task. Or conversely, if you recall an old conversation about meeting for dinner at a restaurant, and this retrieval is confounded with encoding and stored as if it were a new conversation, you might go to the restaurant instead of going

home. These examples show how critical the separation of encoding and retrieval can be for effective network function.

Theta phase precession in CA1

Hippocampal place cells have been shown to systematically shift their phase of firing to earlier phases of the theta rhythm as the animal is exploring an environment (a phenomenon known as theta phase precession) (O'Keefe and Recce, 1993; Skaggs et al., 1996). To remind our readers the observed properties of the theta phase precessed place cells are: (1) all place cells start firing at the same initial phase (O'Keefe and Recce, 1993); (2) the initial phase is on average the same on each entry of the rat into the place field of a place cell; (3) the total amount of phase precession is always less than 360° (O'Keefe and Recce, 1993); (4) the firing rate of the place cell increases as the position of the rat in the place field increases, reaching a maximal value at about 200° and beyond this point it decreases again (Harris et al., 2002; Mehta et al., 2002).

Our model showed that theta phase precession in CA1 can be generated only by theta phase precessed CA3 inputs and maintained by the internal CA1 architecture in collaboration with the medial septal inhibition under specific conditions. First, our model showed that in order for the CA1 pyramidal cells (place cells) to phase precess to a full 360° as the rat reaches the end of the place field, then an excitatory phase precessing input (CA3 Schaffer collateral input), should drive not only the PCs, but also the inhibitory interneurons causing them to also precess (i.e. case 4 described in Mechanisms of Theta Phase Precession in CA1 section). An additional phase precessing inhibitory input (MS_{180} and MS_{360}), which inhibits the CA1 inhibitory interneurons, is also required to ensure that the between phase relationships of the PCs and the inhibitory INs during theta, as they have been observed experimentally (Klausberger et al., 2003, 2004; Fuentealba et al., 2008b; Klausberger and Somogyi, 2008), are also maintained. Experimental evidence has shown that layer 2 EC cells are phase precessing, but not the EC layer 3 cells (Hafting et al., 2008; Mizuseki et al., 2009). The EC layer 2 cells drive both the DG and CA3 excitatory cells, which in turn excite the proximal dendrites of the CA1 PCs, whereas the EC layer 3 cells excite only the distal dendrites of the CA1 PCs. Transient disruption of the CA3 input to CA1 PCs has been shown to cause a transient block of their phase precession dynamics (Zugaro et al., 2005). Therefore, our assumption to model only the CA3 input as providing phase precessed input is consistent with the observed experimental findings. In addition, other experimental evidence has shown that during spatial exploratory behaviour on a linear track, inhibitory interneurons also show phase precession dynamics (Maurer et al., 2006; Ego-Stengel and Wilson, 2007). This finding supports our assumption that also the CA1 inhibitory interneurons should be driven by the CA3 phase precessing input causing them to precess.

Second, our model showed that in order for the firing rate of the place cells to increase as the rat moves through the place field reaching a maximum value at about 200°, beyond which,

it decreases again (Harris et al., 2002; Mehta et al., 2002), then the pyramidal cells (place cells) must increase and decrease their firing activity only when: (1) a CA3 phase precessed input is presented to both CA1 PCs and INs, whose frequency linearly increased from the start till the middle of the place field and subsequently decreased linearly by the same amount till the end of the field; and (2) the CA3 phase precessed input was presented in conjunction with a phase precessed septal and presynaptic $GABA_B$ inhibition to CA1 INs and PCs, respectively, but with constant frequency. As before, because the CA1 inhibitory interneurons were excited by the CA3 phase precessed input (Mizuseki et al., 2009) and a phase precessed septal inhibitory input, then their phase relationships with the CA1 pyramidal cells with respect to theta are maintained (Klausberger et al., 2003, 2004; Klausberger and Somogyi, 2008). Furthermore, the model CA1 inhibitory interneurons' firing activity phase precessed to earlier phases of theta as the rat transversed the place field (Maurer et al., 2006; Ego-Stengel and Wilson, 2007).

Finally, our model showed that in order for the firing rate of a place cell to increase as the position of the rat in the place field increases, reaching a maximal value at about 200° and beyond this point to decrease again (Harris et al., 2002; Mehta et al., 2002), then the CA1 PC proximal synapse must be slightly depressed (see Fig. 12B), thus preventing the firing activity of the PCs to continuously increase as the rat approached the end of the field and to remain anchored to the end of the theta cycle (as in case 1 from the Mechanisms of Theta Phase Precession in CA1 section).

What is Next?

Several extensions to the basic idea deserve further consideration. One such idea is to scale up the network to match the relative percentages of excitatory and inhibitory cells in CA1 [i.e. 90% excitatory cells and 10% inhibitory cells (Vida, 2010)]. Within the population of inhibitory cells, BC, BSC, and AAC may represent 60%, 25%, and 15% of the population (Baude et al., 2007). Scaling up our network model will allow us to circumvent the case of a single theta phase precessing interneuron inhibiting pyramidal cells with place fields at different and overlapping locations, thus simultaneously inhibiting pyramidal cells that are at different stages (i.e., theta phases) of phase precession. In this case, a single theta phase precessing interneuron may only correctly time only a few of its postsynaptic pyramidal cells. However, if our scaled up network consisted of, for example, 400 PCs and 24 inhibitory interneurons (i.e. less than 10% inhibition), with each set of 100 PCs and 6 INs representing a microcircuit coding for a spatial location, driven by EC and CA3 inputs presented at different, but overlapping times, then the potentially simultaneous inhibition of PCs at different stages (i.e. theta phases) of phase precession maybe overcome.

Another idea is to test the robustness of the scaled up model. How would the firing patterns of CA1 interneurons and place cells change with more realistic, noisy, input coming from mul-

tiple EC and CA3 cells? How would random synaptic delays affect the results? How will the results scale with noise in connectivity parameters?

Finally, a future project could address how cholinergic and GABAergic neurons from the medial septum facilitate (or do not facilitate) the encoding, storage, and replay of place-cell memories in the hippocampus, subiculum, and entorhinal cortex during active waking, quiet waking, and slow wave sleep in the presence of various types of inhibitory interneurons. Hasselmo (1999) proposed a conceptual model of the two-stage memory formation model (Buzsaki, 1989) in the presence of low and high levels of acetylcholine (ACh). According to this model (Hasselmo et al., 1996; Hasselmo, 1999) "the high levels of ACh, which are present during active waking might set the appropriate dynamics for encoding new information in the hippocampus, by partially suppressing excitatory feedback connections and so facilitating encoding without interference from previously stored information." On the other hand, when ACh levels are low during quite waking and slow-wave sleep, this suppression is released allowing a stronger spread of hippocampal activity to reach the entorhinal cortex and neocortex, thus facilitating the process of consolidation of separate memory traces. However, when this model (Hasselmo, 1999) was proposed very little was known about the firing properties of inhibitory interneurons in the hippocampus and medial septum during theta and sharp-wave ripple activity. The dramatic expansion of our knowledge about the anatomical, physiological, and molecular characteristics as well as the connectivity and synaptic properties of various inhibitory cell types (both local and long-range) in the hippocampal and septal microcircuits (Cutsuridis et al., 2010) will allow us to decipher the biophysical computations of information processing therein during waking and slow wave sleep.

REFERENCES

Alonso A, García-Austt E. 1987. Neuronal sources of theta rhythm in the entorhinal cortex of the rat. II. Phase relations between unit discharges and theta field potentials. Exp Brain Res 67:502–509

Ascoli GA, Alonso-Nanclares L, Anderson SA, Barrionuevo G, Benavides-Piccione R, Burkhalter A, Buzsáki G, Cauli B, Defelipe J, Fairén A, Feldmeyer D, Fishell G, Fregnac Y, Freund TF, Gardner D, Gardner EP, Goldberg JH, Helmstaedter M, Hestrin S, Karube F, Kisvárday ZF, Lambolez B, Lewis DA, Marin O, Markram H, Muñoz A, Packer A, Petersen CC, Rockland KS, Rossier J, Rudy B, Somogyi P, Staiger JF, Tamas G, Thomson AM, Toledo-Rodriguez M, Wang Y, West DC, Yuste R. 2008. Petilla terminology: Nomenclature of features of GABAergic interneurons of the cerebral cortex. Nat Rev Neurosci 9:557–568.

Baude A, Bleasdale C, Dalezios Y, Somogyi P, Klausberger T. 2007. Immunoreactivity for the GABAA receptor alpha1 subunit, somatostatin and Connexin36 distinguishes axoaxonic, basket, and bistratified interneurons of the rat hippocampus. Cereb Cortex 17:2094–2107.

Borhegyi Z, Varga V, Szilagyi N, Fabo D, Freund TF. 2004. Phase segregation of medial septal GABAergic neurons during hippocampal theta activity. J Neurosci 24:8470–8479.

Brankack J, Stewart M, Fox SE. 1993. Current source density analysis of the hippocampal theta rhythm: Associated sustained potentials and candidate synaptic generators. Brain Res 615:310–327.

Brun VH, Leutgeb S, Wu HQ, Schwarcz R, Witter MP, Moser EI, Moser MB. 2008. Impaired spatial representation in CA1 after lesion of direct input from entorhinal cortex. Neuron 57:290–302.

Brun VH, Otnass MK, Molden S, Steffenach HA, Witter MP, Moser MB, Moser EI. 2002. Place cells and place recognition maintained by direct entorhinal-hippocampal circuitry. Science 296:2243–2246.

Buzsaki G. 1989. Two stage model of memory trace formation: A role for "noisy" brain states. Neuroscience 31:551–570.

Buzsaki G. 2002. Theta oscillations in the hippocampus. Neuron 33:325–340.

Capogna M. 2011. Neurogliaform cells and other interneurons of stratum lacunosum-moleculare gate entorhinal-hippocampal dialogue. J Physiol 589:1875–1883.

Cobb S, Lawrence JJ. 2010. Neuromodulation of hippocampal cells and circuits. In: Cutsuridis V, et al., editors.Hippocampal Microcircuits: A Computational Modeller's Resource Book, Vol. V. New York: Springer. pp 187–246.

Cobb S, Vida I. 2010. Neuronal activity patterns in anaesthetized animals. In: Cutsuridis V, et al., editors.Hippocampal Microcircuits: A Computational Modeler's Resource Book, Vol. V. New York: Springer. pp 277–291.

Colgin LL, Denninger T, Fyhn M, Hafting T, Bonnevie T, Jensen O, Moser MB, Moser EI. 2009. Frequency of gamma oscillations routes flow of information in the hippocampus. Nature 462:353–358.

Cutsuridis V, Cobb S, Graham BP. 2008. Encoding and retrieval in a CA1 microcircuit model of the hippocampus. In: Kurkova V, et al., editors. Lecture Notes in Computer Science 5164. Berlin Heidelberg: Springer-Verlag. pp 238–247.

Cutsuridis V, Cobb S, Graham BP. 2010a. Encoding and retrieval in the hippocampal CA1 microcircuit model. Hippocampus 20:423–446.

Cutsuridis V, Graham BP, Cobb S, Hasselmo M. 2011. Bio-inspired models of memory capacity, recall performance and theta phase precession. In: IJCNN 2011, San Hose, CA, July 31 to August 5, 2011.

Cutsuridis V, Graham BP, Cobb S, Vida I. 2010b. Hippocampal Microcircuits: A Computational Modeler's Resource Book. New York: Springer.

Cutsuridis V, Hasselmo M. 2010. Dynamics and function of a CA1 model of the hippocampus during theta and ripples. In: Diamantaras K, Duch W, Iliadis LS, editors. ICANN 2010, Part I, LNCS 6352. Berlin Heidelberg: Springer-Verlag. pp 230–240.

Cutsuridis V, Kahramanoglou I, Smyrnis N, Evdokimidis I, Perantonis S. 2007. A neural variable integrator model of decision making in an antisaccade task. Neurocomputing 70:1390–1402.

Cutsuridis V, Wennekers T. 2009. Hippocampus, microcircuits and associative memory. Neural Netw 22:1120–1128.

Dragoi G, Carpi D, Recce M, Csicsvari J, Buzsaki G. 1999. Interactions between hippocampus and medial septum during sharp waves and theta oscillation in the behaving rat. J Neurosci 19:6191–6199.

Ego-Stengel V, Wilson MA. 2007. Spatial selectivity and theta phase precession in CA1 interneurons. Hippocampus 17:161–174.

Ermentrout B. 2002. Simulating, Analyzing, and Animating Dynamical Systems: A Guide to XPPAUT for Researchers and Students (SIAM).

Fox SE, Wolfson S, Ranck JB Jr. 1986. Hippocampal theta rhythm and the firing of neurons in walking and urethane anesthetized rats. Exp Brain Res 62,495–508.

Freund TF. 1989. GABAergic septohippocampal neurons contain parvalbumin. Brain Res 478:375–381.

Freund TF, Antal M. 1988. GABA-containing neurons in the septum control inhibitory interneurons in the hippocampus. Nature 336:170–173.

Fuentealba P, Begum R, Capogna M, Jinno S, Márton LF, Csicsvari J, Thomson A, Somogyi P, Klausberger T. 2008a. Ivy cells: A population of nitric-oxide-producing, slow-spiking GABAergic neurons and their involvement in hippocampal network activity. Neuron 57:917–929.

Fuentealba P, Klausberger T, Karayannis T, Suen WY, Huck J, Tomioka R, Rockland K, Capogna M, Studer M, Morales M, Somogyi P. 2010. Expression of COUP-TFII nuclear receptor in restricted GABAergic neuronal populations in the adult rat hippocampus. J. Neurosci 30:1595–1609.

Fuentealba P, Tomioka R, Dalezios Y, Márton LF, Studet M, Rockland K, Klausberger T, Somogyi P. 2008b. Rhythmically active enkephalin-expressing GABAergic cells in the CA1 area of the hippocampus project to the subiculum and preferentially innervate interneurons. J Neurosci 28:10017–10022.

Gasbarri A, Sulli A, Packard MG. 1997. The dopaminergic mesencephalic projections to the hippocampal formation in the rat. Prog Neuropsychopharmacol Biol Psychiatry 21:1–22.

Gasparini S, Magee JC. 2006. State-dependent dendritic computation in hippocampal CA1 pyramidal neurons. J Neurosci 26:2088–2100.

Geisler C, Diba K, Pastalkova E, Mizuseki K, Royer S, Buzsáki G. 2010. Temporal delays among place cells determine the frequency of population theta oscillations in the hippocampus. Proc Natl Acad Sci USA 107:7957–7962.

Hafting T, Fynn M, Bonnevie T, Moser MB, Moser EI. 2008. Hippocampus-independent phase precession in entorhinal grid cells. Nature 453:1248–1252.

Harris KD, Henze DA, Hirase H, Leinekugel Z, Dragoi G, Czurko A, Buzsaki G. 2002. Spike train dynamics predicts theta-related phase precession in hippocampal pyramidal cells. Nature 417:738–741.

Harvey CD, Collman F, Dombeck DA, Tank DW. 2009. Intracellular dynamics of hippocampal place cells during virtual navigation. Nature 461:941–946.

Hasselmo ME. 1999. Neuromodulation: Acetylcholine and memory consolidation. Trends Cogn Sci 3:351–359.

Hasselmo M, Bodelon C, Wyble B. 2002. A proposed function of the hippocampal theta rhythm: Separate phases of encoding and retrieval enhance reversal of prior learning. Neural Comput 14:793–817.

Hasselmo M, Schnell E. 1994. Laminar selectivity of the cholinergic suppression of synaptic transmission in rat hippocampal region CA1: Computational modelling and brain slice physiology. J Neurosci 14:3898–3914.

Hasselmo ME, Wyble BP, Wallenstein GV. 1996. Encoding and retrieval of episodic memories: Role of cholinergic and GABAergic modulation in the hippocampus. Hippocampus 6:693–708.

Ito HT, Schuman EM. 2007. Frequency-dependent gating of synaptic transmission and plasticity by dopamine. Front Neural Circuits 1:1–13.

Jarsky T, Roxin A, Kath WL, Spruston N. 2005. Conditional dendritic spike propagation following distal synaptic activation of hippocampal CA1 pyramidal neurons. Nat Neurosci 8:1667–1676.

Jensen O, Lisman JE. 1996. Hippocampal CA3 region predicts memory sequences: Accounting for the phase precession of place cells. Learn Mem 3:279–287.

Jinno S, Klausberger T, Marton LF, Dalezios Y, Roberts JD, Fuentealba P, Bushong EA, Henze D, Buzsáki G, Somogyi P. 2007. Neuronal diversity in GABAergic long-range projections from the hippocampus. J Neurosci 27:8790–804.

Johnson A, Redish AD. 2007. Neural ensembles in CA3 transiently encode paths forward of the animal at a decision point. J Neurosci 27:12176–12189.

Kamondi A, Acsady L, Wang XJ, Buzsaki G. 1998. Theta oscillations in somata and dendrites of hippocampal pyramidal cells in vivo: Activity-dependent phase precession of action potentials. Hippocampus 8:244–261.

Klausberger T. 2009. GABAergic interneurons targeting dendrites of pyramidal cells in the CA1 area of the hippocampus. Eur J Neurosci 30:947–957.

Klausberger T, Magill PJ, Marton LF, David J, Roberts B, Cobden PM, Buzsaki G, Somogyi P. 2003. Brain-state- and cell-type-specific firing of hippocampal interneurons in vivo. Nature 421:844–848.

Klausberger T, Marton LF, Baude A, Roberts JD, Magill PJ, Somogyi P. 2004. Spike timing of dendrite-targeting bistratified cells during hippocampal network oscillations in vivo. Nat Neurosci 7:41–47.

Klausberger T, Marton LF, O'Neill J, Huck JH, Dalezios Y, Fuentealba P, Suen WY, Papp E, Kaneko T, Watanabe M, Csicsvari J, Somogyi P. 2005. Complementary roles of cholecystokinin- and parvalbumin-expressing GABAergic neurons in hippocampal network oscillations. J Neurosci 25:9782–9793.

Klausberger T, Somogyi P. 2008. Neuronal diversity and temporal dynamics: The unity of hippocampal circuit operations. Science 321:53–57.

Lee I, Kesner RP. 2004. Differential contributions of dorsal hippocampal subregions to memory acquisition and retrieval in contextual-fear conditioning. Hippocampus 14:301–310.

Lengyel M, Szatmary Z, Erdi P. 2003. Dynamically detuned oscillations account for the coupled rate and temporal code of place cell firing. Hippocampus 13:700–714.

Magee JC. 2001. Dendritic mechanisms of phase precession in hippocampal CA1 pyramidal neurons. J Neurophysiol 86:528–532.

Maurer AP, Cowen SL, Burke SN, Barnes CA, McNaughton BL. 2006. Phase precession in hippocampal interneurons showing strong functional coupling to individual pyramidal cells. J Neurosci 26:13485–13492.

Maurer AP, McNaughton BL. 2007. Network and intrinsic cellular mechanisms underlying theta phase precession of hippocampal neurons. Trends Neurosci 30:325–333.

Mehta MR, Lee AK, Wilson MA. 2002. Role of experience and oscillations in transforming a rate code into a temporal code. Nature 417:741–746.

Mizuseki K, Sirota A, Pastalkova E, Buzsaki G. 2009. Theta oscillations provide temporal windows for local circuit computation in the entorhinal-hippocampal loop. Neuron 64:267–280.

Molyneaux BJ, Hasselmo M. 2002. GABA$_B$ presynaptic inhibition has an in vivo time constant sufficiently rapid to allow modulation at theta frequency. J Neurophys 87:1196–1205.

O'Keefe J, Burgess N. 2005. Dual phase and rate coding in hippocampal place cells: Theoretical significance and relationship to entorhinal grid cells. Hippocampus 15:853–866.

O'Keefe J, Recce ML. 1993. Phase relationship between hippocampal place units and the EEG theta rhythm. Hippocampus 3:317–330.

Otmakhova NA, Lisman JE. 1999. Dopamine selectively inhibits the direct cortical pathway to the CA1 hippocampal region. J Neurosci 19:1437–1445.

Rubin JE, Gerkin RC, Bi GQ, Chow CC. 2005. Calcium time course as signal for spike-timing-dependent plasticity. J Neurophysiol 93:2600–2613.

Skaggs WE, McNaughton BL, Wilson MA, Barnes CA. 1996. Theta phase precession in hippocampal neuronal populations and the compression of temporal sequences. Hippocampus 6:149–172.

Somogyi P, Klausberger T. 2005. Defined types of cortical interneurons structure space and spike timing in the hippocampus. J Physiol 562:9–26.

Thurley K, Leibold C, Gundlfinger A, Schmitz D, Kempter R. 2008. Phase precession through synaptic facilitation. Neural Comput 20:1285–1324.

Toth K, Borhegyi Z, Freund TF. 1993. Postsynaptic targets of GABAergic hippocampal neurons in the medial septum-diagonal band of Broca complex. J Neurosci 13:3712–3724.

Tsodyks MV, Skaggs WE, Sejnowski TJ, McNaughton BL. 1996. Population dynamics and theta rhythm phase precession of hippocampal place cell firing: A spiking neuron model. Hippocampus 6:271–280.

Vertes RP, Kocsis B. 1997. Brainstem–diencephalo–septohippocampal systems controlling the theta rhythm of the hippocampus. Neuroscience 81:893–926.

Vida I. 2010. Morphology of hippocampal neurons. In: Cutsuridis V, et al. editors. Hippocampal Microcircuits: A Computational Modeler's Resource Book. New York: Springer. pp 27–67.

Vinogradova O. 2001. Hippocampus as a comparator: Role of the two input and two output systems of the hippocampus in selection and registration of information. Hippocampus 11:578–598.

Wallenstein GV, Hasselmo ME. 1997. GABArgic modulation of hippocampal population activity: Sequence learning, place field development and the phase precession effect. J. Neurophys 78:393–408.

Wilson MA, McNaughton BL. 1993. Dynamics of the hippocampal ensemble code for space. Science 261:1055–1058.

Winson J. 1978. Loss of hippocampal theta rhythm results in spatial memory deficit in the rat. Science 210:160–163.

Witter M. 2010. Connectivity of the hippocampus. In: Cutsuridis V, et al. editors. Hippocampal Microcircuits: A Computational Modeler's Resource Book. New York: Springer. pp 5–26.

Zugaro MB, Monconduit L, Buzsaki G. 2005. Spike phase precession persists after transient intrahippocampal perturbation. Nat Neurosci 8:67–71.

APPENDIX: MATHEMATICAL FORMALISM

This appendix contains the mathematical formalisms of the model cell types. Simulations were performed using the XPPAUT (Ermentrout, 2002). Data analysis was performed by MATLAB. Parameter units are measured in mV for potentials, $\mu A/cm^2$ for applied currents, mS/cm^2 for maximal conductances, and $\mu F/cm^2$ for capacitances.

CA1 Pyramidal Cell

The axonic (ax), somatic (s), proximal dendritic (pd), and distal dendritic (dd) compartments of the pyramidal neuron obey the following current balance equations

$$C_m \frac{dV_{ax}}{dt} = I_L + I_{Na,ax} + I_{K,ax} + I_{coup} + I_{syn} + I_{in} \quad (A1)$$

$$C_m \frac{dV_s}{dt} = I_L + I_{Na,s} + I_{K_{dr,s}} + I_{A,s} + I_{m,AHAP,s} + I_{CaL,s} \\ + I_h + I_{coup} + I_{syn} + I_{in} \quad (A2)$$

$$C_m \frac{dV_{pd}}{dt} = I_L + I_{Na,d} + I_{K_{dr,d}} + I_{A,d} + I_{CaL,d} + I_h + I_{coup} + I_{syn} + I_{in} \quad (A3)$$

$$C_m \frac{dV_{dd}}{dt} = I_L + I_{Na,d} + I_{K_{dr,d}} + I_{A,d} + I_{CaL,d} + I_h + I_{coup} + I_{syn} + I_{in} \quad (A4)$$

where I_L is the leak current, I_{Na} is the sodium current, I_K is the delayed rectifier potassium current, I_A is the type A potassium current, $I_{m,AHP}$ is the medium Ca^{2+}-activated K^+ afterhyperpolarization current, I_{CaL} is the L-type Ca^{2+} current, I_h is the h-current, I_{coup} is the electrical coupling between compartments, I_{in} is the injected current, and I_{syn} is the synaptic current. Table A2 displays the ionic parameter values of the CA1 pyramidal cell.

The coupling currents for all compartments are

$$I_{coup}^{axon} = g_{axon,soma} \cdot (V_{soma} - V_{axon}) \quad (A5)$$

$$I_{coup}^{soma} = g_{soma,axon} \cdot (V_{axon} - V_{soma}) + g_{soma,dend_{prox}} \cdot (V_{pd} - V_{soma}) \quad (A6)$$

$$I_{coup}^{dend_{prox}} = g_{soma,dend_{prox}} \cdot (V_{soma} - V_{pd}) + g_{dend_{dist},dend_{prox}}(V_{dd} - V_{pd}) \quad (A7)$$

$$I_{coup}^{dend_{dist}} = g_{dend_{prox},dend_{dist}}(V_{pd} - V_{dd}) \quad (A8)$$

The leak current is described by

$$I_L = g_L \cdot (V - V_L) \quad (A9)$$

where g_L is the leak conductance and V_L is the leak reversal potential.

The sodium current at the axon and soma is described by:

$$I_{Na} = -g_{Na} \cdot M_{Na}^2 \cdot H_{Na} \cdot (V - V_{Na}) \quad (A10)$$

where g_{Na} is the maximal conductance of the Na^+ current, M_{Na} and H_{Na} are the activation and inactivation constants and V_{Na} is the reversal potential of the Na^+ current. The activation and inactivation constants at the soma are given by

$$M_{Na} = \alpha_M(V)/(\alpha_M(V) + \beta_M(V))$$
$$\alpha_M(V) = 0.32 \cdot (-46.9 - V)/(\exp((-46.9 - V)/4.0) - 1.0)$$
$$\beta_M(V) = 0.28 \cdot (V + 19.9)/(\exp((V + 19.9)/5.0) - 1.0)$$
$$H_{Na}' = \alpha_H(V) - (\alpha_H(V) + \beta_H(V)) \cdot H_{Na}$$
$$\alpha_H(V) = 0.128 \cdot \exp((-43 - V)/18)$$
$$\beta_H(V) = 4/(1 + \exp((-20 - V)/5))$$

TABLE A1.

Synaptic Strength Parameter Values

Name	Value theta	Name	Value theta
$w_{ec\text{-to-pcAMPA}}$	$1.4 + W_3$	$w_{aac\text{-to-pc}}$	1.0
$w_{ca3\text{-to-pcAMPA}}$	$2.4 + W_1$	$w_{bc\text{-to-pc}}$	0.1
$w_{ec\text{-to-pcNMDA}}$	$1.4 + W_3$	$w_{bc\text{-to-bsc}}$	20
$w_{ca3\text{-to-pcNMDA}}$	$2.4 + W_1$	$w_{bsc\text{-to-pc}}$	0.3
$w_{ec\text{-to-aac}}$	0.9	$w_{pc\text{-to-bsc}}$	0
$w_{ca3\text{-to-aac}}$	0.8	$w_{bsc\text{-to-bc}}$	0.5
$w_{ec\text{-to-bc}}$	0.8	$w_{olm\text{-to-pc}}$	0.5
$w_{ca3\text{-to-bc}}$	0.8	$w_{pc\text{-to-olm}}$	1.1
$w_{ca3\text{-to-bsc}}$	2	$w_{ivy\text{-to-pc}}$	0.15
$w_{sep360\text{-to-aac}}$	10	$w_{pc\text{-to-ivy}}$	1
$w_{sep360\text{-to-bc}}$	10	$w_{ec\text{-to-ngl}}$	3
$w_{sep180\text{-to-bsc}}$	8	$w_{ngl\text{-to-pc}}$	0.8
$w_{sep180\text{-to-olm}}$	30	$w_{bc\text{-to-pc}}$	0.1
$w_{OLM\text{-to-NGL}}$	1,500		

TABLE A2. ━━━━━━━━━━━

Pyramidal cell parameter values

Name	Value	Name	Value
C_m	1	$g_{A,dend}$	12
g_L	0.1	asap	0.001
V_L	−70	ζ_p	30
g_{coup}	1.125	inact	72
$g_{Na,soma}$	30	$inact_2$	0.11
$g_{Na,axon}$	100	$inact_3$	2
V_{Na}	60	$inact_4$	64
$g_{Na,dend}$	30	$inact_5$	1
natt	0	$g_{K,dr,axon}$	20
T	23	$g_{K,dr,soma}$	14
$g_{A,soma}$	7.5	$g_{K,dr,dend}$	14
g_{mAHP}	25	V_k	−80
qhat	1	qma	0.00048
qmb	0.28	β_s	0.083
$g_{CaL,soma}$	7	β_d	0.083
$g_{CaL,dend}$	25	s	0
V_{Ca}	140	nonc	6
Ca^{2+}	2	Ca_τ	1,000
φ_s	0.1	s_1	0
φ_d	0.1	s_2	40
$\chi_{0,s}$	0.05	s_3	3.6
$\chi_{0,d}$	0.07	Mg^{2+}	2
κ	7		

Units: g, mS/cm^2; C_m, μF/cm^2; V, mV; T, Celsius.

The sodium current at the dendrite is described by:

$$I_{Na,d} = -g_{Na,d} \cdot M_{Na,d}^2 \cdot H_{Na,d} \cdot D_{Na,d} \cdot (V_d - V_{Na}) \quad (A11)$$

where

$$M'_{Na,d} = (M_{\infty_{Na,d}} - M_{Na,d})/\tau_{M_{Na,d}}$$
$$M_{\infty_{Na,d}} = 1/(1 + \exp((-V_d - 40)/3))$$
$$\tau_{M_{Na,d}} = 0.1$$
$$H'_{Na,d} = (H_{\infty_{Na,d}} - H_{Na,d})/\tau_{H_{Na,d}}$$
$$H_{\infty_{Na,d}} = 1/(1 + \exp((V_d + 45)/3))$$
$$\tau_{H_{Na,d}} = 0.5$$
$$D'_{Na,d} = (D_{\infty_{Na,d}} - D_{Na,d})/\tau_{D_{Na,d}}$$
$$D_{\infty_{Na,d}} = (1 + natt \cdot \exp((V_d + 60)/2))/(1 + \exp((V_d + 60)/2))$$
$$\tau_{D_{Na,d}} = \max(0.1, (0.00333 \cdot \exp(0.0024 \cdot (V_d + 60) \cdot Q))/$$
$$(1 + \exp(0.0012 \cdot (V_d + 60) \cdot Q)))$$
$$Q = 96480/(8.315 \cdot (273.16° + T))$$

where T is the temperature in Celsius and natt is the Na$^+$ attenuation. The type-A K$^+$ current at the soma and dendrite is given by

$$I_{K_{A,d}} = -g_{K_{A,d}} \cdot A_d \cdot B_d \cdot (V_d - V_K) \quad (A12)$$

The activation and inactivation constants are given by

$$A'_d = (A_{\infty_d} - A_d)/\tau_{A_d}$$
$$A_{\infty_d} = 1/(1 + A_{\alpha,d})$$
$$A_{\alpha,d} = \exp(asap \cdot \varsigma(V_d) \cdot (V_d + 1) \cdot Q)$$
$$A_{\beta,d} = \exp(0.00039 \cdot Q \cdot (V_d + 1) \cdot \varsigma_2(V_d))$$
$$\tau_{A_d} = \max(A_{\beta,d}/((1 + A_{\alpha,d}) \cdot QT \cdot 0.1), \ 0.1)$$
$$\varsigma(V_d) = -1.5 - (1/(1 + \exp((V_d + \varsigma_p)/5)))$$
$$\varsigma_2(V_d) = -1.8 - (1/(1 + \exp((V_d + 40)/5)))$$
$$B'_d = (B_{\infty_d} - B_d)/\tau_{B_d}$$
$$B_{\infty_d} = 0.3 + 0.7/(1 + \exp(inact_2 \cdot (V_s + inact) \cdot Q))$$
$$\tau_{B_d} = \kappa \cdot \max(inact_3 \cdot (V_s + inact_4), inact_5)$$

The delayed rectifier K$^+$ current at the axon and soma is given by

$$I_{K_{dr}} = -g_{K_{dr}} \cdot N \cdot (V - V_K) \quad (A13)$$

where g_{Kds} is the maximal conductance. The activation constant, N is given by

$$N' = \alpha_N(V) - (\alpha_N(V) + \beta_N(V)) \cdot N$$
$$\alpha_N(V) = 0.016 \cdot (-24.9 - V)/(\exp((-24.9 - V)/5) - 1)$$
$$\beta_N(V) = 0.25 \cdot \exp(-1 - 0.025 \cdot V)$$

The delayed rectifier K$^+$ current at the dendrite is given by

$$I_{K_{dr,d}} = -g_{K_{dr,d}} \cdot N_d^2 \cdot (V_d - V_K) \quad (A14)$$

where $g_{Kdr,d}$ is the maximal conductance. The activation constant, N_d is given by

$$N'_d = (N_{\infty_d} - N_d)/\tau_{N_d}$$
$$N_{\infty_d} = 1/(1 + \exp((-V_d - 42)/2))$$
$$\tau_{N_d} = 2.2$$

The medium Ca^{2+}-activated K$^+$ afterhyperpolarization current at the soma is given by

$$I_{mAHP} = -g_{mAHP} \cdot Q_m \cdot (V_s - V_K) \quad (A14a)$$

where g_{KmAHP} is the maximal conductance. The activation constant, Q_m is given by

$$Q'_m = (Q_{m_\infty} - Q_m)/\tau_{Q_m}$$
$$Q_{m_\infty} = qhat \cdot Q_{m_\alpha} \cdot \tau_{Q_m}$$
$$Q_{m_\alpha} = qma \cdot \chi_s/(0.001 \cdot \chi_s + 0.18 \cdot \exp(-1.68 \cdot V_s \cdot Q))$$
$$Q_{m_\beta} = (qmb \cdot \exp(-0.022 \cdot V_s \cdot Q))/(\exp(-0.022 \cdot V_s \cdot Q) + 0.001 \cdot \chi_s)$$
$$\tau_{Q_m} = 1/(Q_{m_\alpha} + Q_{m_\beta})$$

The h-current (Cutsuridis et al., 2010) at the soma and dendrite is described by

$$I_h = -g_h \cdot tt \cdot (V - E_h) \tag{A15}$$

$$\frac{dtt}{dt} = \frac{tt_\infty - tt}{\tau_{tt}}$$

$$tt_\infty = \frac{1}{1 + e^{-(V - V_{halft})/k_l}} \qquad \tau_{tt} = \frac{e^{0.0378 \cdot \varsigma \cdot gmt \cdot (V - V_{halft})}}{qtl \cdot q10^{(T-33)/10} \cdot a0t \cdot (1 + a_{tt})}$$

$$a_{tt} = e^{0.00378 \cdot \varsigma \cdot (V - V_{halft})}$$

where g_h is the maximal conductance of the h-current and E_h is the reversal potential. The L-type Ca^{2+} current at the soma is described by

$$I_{CaL_s} = -g_{CaL_s} \cdot S_s \cdot g_{hk}(V_s, \chi_s) \cdot (1/(1 + \chi_s)) \tag{A16}$$

where $g_{CaL,s}$ is the maximal conductance and

$$S'_s = (S_{\infty_s} - S_s)/\tau_{s_s}$$

$$S_{\infty_s} = \alpha_s(V_s)/(\alpha_a(V_s) + \beta_s(V_s))$$

$$\tau_{s_s} = 1/(5 \cdot (\alpha_s(V_s) + \beta_s(V_s)))$$

$$\alpha_s(V_s) = -0.055 \cdot (V_s + 27.01)/(\exp((-V_s - 27.01)/3.8) - 1)$$

$$\beta_s(V_s) = 0.94 \cdot \exp((-V_s - 63.01)/17)$$

$$xx = 0.0853 \cdot (273.16 + T)/2$$

$$f(z) = (1 - z/2) \cdot f_2(z) + (z/(\exp(z) - 1)) \cdot f_3(z)$$

$$f_2(z) = H(0.0001 - |z|)$$

$$f_3(z) = H(|z| - 0.0001)$$

$$g_{hk} = -xx \cdot (1 - ((\chi_s/Ca) \cdot \exp(V_s/xx))) \cdot f(V_s/xx)$$

The Ca^{2+} concentrations in the soma and dendrites are given by

$$\chi'_s = \phi_s \cdot I_{CaL_s} - (\beta_s \cdot (\chi_s - \chi_{0,s})) + (\chi_{pd} - \chi_s)/Ca_\tau - (\beta_s/nonc) \cdot \chi_s^2 \tag{A17}$$

$$\chi'_{pd} = \phi_d \cdot (I_{CaL_d} + I_{Ca,NMDA}) - \beta_d \cdot (\chi_{pd} - \chi_{0,d}) - (\beta_d/nonc) \cdot \chi_{pd}^2 - buff \cdot \chi_{pd} \tag{A18}$$

$$\chi'_{dd} = \phi_d \cdot (I_{CaL_d} + I_{Ca,NMDA}) - \beta_d \cdot (\chi_{dd} - \chi_{0,d}) - (\beta_d/nonc) \cdot \chi_{dd}^2 - buff \cdot \chi_{dd} \tag{A19}$$

The L-type Ca^{2+} current at the dendrite is described by

$$I_{CaL_d} = -g_{CaL_d} \cdot S_d^3 \cdot T_d \cdot (V_d - V_{Ca}) \tag{A20}$$

Hippocampus

$$S'_d = (S_{\infty_d} - S_d)/\tau_{s_d}$$

$$S_{\infty_d} = 1/(1 + \exp(-V_d - 37))$$

$$\tau_{s_d} = s_3 + s_1/(1 + \exp(V_d + s_2))$$

$$T'_d = (T_{\infty_d} - T_d)/\tau_{T_d}$$

$$T_{\infty_d} = 1/(1 + \exp((V_d + 41)/0.5))$$

$$\tau_{T_d} = 29$$

The calcium detector model is governed by the following six equations:

$$P' = (\phi_a(\chi_d) - c_p \cdot A \cdot P)/\tau_p \tag{A21}$$

$$V' = (\phi_b(\chi_d) - V)/\tau_V \tag{A22}$$

$$A' = (\phi_c(\chi_d) - A)/\tau_A \tag{A23}$$

$$B' = (\phi_e(A) - B - c_d \cdot B \cdot V)/\tau_b \tag{A24}$$

$$D' = (\phi_d(B) - D)/\tau_D \tag{A25}$$

$$W' = (\alpha_w/(1 + \exp((P - a)/p_a)) - \beta_w/(1 + (\exp((D - d)/p_d)) - W)/\tau_w \tag{A26}$$

where P is the potentiation detector dynamics, V is the veto detector dynamics, D is the depression detector dynamics, A and B are the intermediate steps leading up to D and W is the readout variable (see Fig. 2). The Hill equations are

$$\phi_a(x) = num_a \cdot ((x/CmHC)^{CmHN})/(1 + (x/CmHC)^{CmHN})$$

$$\phi_b(x) = num_b \cdot ((x/CnHC)^{CnHN})/(1 + (x/CnHC)^{CnHN})$$

$$\phi_c(x) = num_c/(1 + \exp((x - \theta_c)/\sigma_c))$$

$$\phi_d(x) = num_d/(1 + \exp((x - \theta_d)/\sigma_d))$$

$$\phi_e(x) = num_e/(1 + \exp((x - \theta_e)/\sigma_e))$$

The calcium detector parameter values are displayed in Table A3.

Basket, Axoaxonic, Bistratified and Ivy Cells

$$C_m \frac{dV}{dt} = I_L + I_{Na} + I_{K_{dr}} + I_A + I_{in} + I_{syn} \tag{A27}$$

where C_m is the membrane capacitance, V is the membrane potential, I_L is the leak current, I_{Na} is the sodium current, $I_{K_{dr}}$ is the fast delayed rectifier K^+ current, I_A is the A-type K^+ current, and I_{syn} is the synaptic current.

TABLE A3. ━━━━━━━━

Calcium Detector Model Parameter Values

Name	Value	Name	Value
c_P	5	num_b	1
τ_P	500	num_c	1
τ_v	10	num_d	1
τ_A	5	num_e	5
τ_B	40	CmHC	4
τ_D	250	CmHN	4
τ_w	500	CnHC	0.6
α_w	0.8	CnHN	3
β_w	0.6	θ_c	2
a	0.3	θ_d	2.6
p_a	−0.1	θ_e	0.55
d	0.05	σ_c	−0.05
p_d	−0.002	σ_d	−0.01
num_a	10	σ_e	−0.02
c_d	4		

Units: g, mS/cm^2; V, mV; α, 1/ms; β, 1/ms.

The sodium current and its kinetics are described by,

$$I_{Na} = g_{Na}m^3h(V - E_{Na}) \qquad (A28)$$

$$\frac{dm}{dt} = \alpha_m(1 - m) - \beta_m m, \quad \alpha_m = \frac{0.1(V + 40)}{(1 - e^{(V+40)/10})},$$

$$\beta_m = 4 \cdot e^{(-(v+65)/18)}$$

$$\frac{dh}{dt} = \alpha_h(1 - h) - \beta_h h, \quad \alpha_h = 0.07 \cdot e^{-(V+65)/20},$$

$$\beta_h = \frac{1}{(1 + e^{-(V+35)/10})}$$

The fast delayed rectifier K$^+$ current, I_{Kdr} is given by

$$I_{Kdr} = g_{Kdr}n^4(V - E_K) \qquad (A29)$$

$$\frac{dn}{dt} = \alpha_n(1 - n) - \beta_n n, \quad \alpha_n = \frac{0.01(V + 55)}{(1 - e^{-(V+55)/10})},$$

$$\beta_n = 0.125e^{-(v+65)/80}$$

The A-type K$^+$ current, I_A, is described by

$$I_A = g_A ab(V - E_k) \qquad (A30)$$

$$\frac{da}{dt} = \alpha_a(1 - a) - \beta_a a, \quad \alpha_a = \frac{0.02(13.1 - V)}{e^{\left(\frac{13.1-V}{10}\right)} - 1},$$

$$\beta_a = \frac{0.0175(V - 40.1)}{e^{\left(\frac{V-40.1}{10}\right)} - 1}$$

$$\frac{db}{dt} = \alpha_b(1 - b) - \beta_b b, \quad \alpha_b = 0.0016e^{\left(\frac{-13-V}{18}\right)}. \quad \beta_b = \frac{0.05}{1 + e^{\left(\frac{10.1-V}{5}\right)}}$$

The ionic parameter values are depicted in Table A4.

Neurogliaform Cell

$$C_m \frac{dV}{dt} = I_L + I_{Na} + I_{K_{dr}} + I_{in} + I_{syn} \qquad (A31)$$

where C_m is the membrane capacitance, V is the membrane potential, I_L is the leak current, I_{Na} is the sodium current, I_{Kdr} is the fast delayed rectifier K$^+$ current, and I_{syn} is the synaptic current.

The sodium current and its kinetics are described by,

$$I_{Na} = g_{Na}m^3h(V - E_{Na}) \qquad (A32)$$

$$\frac{dm}{dt} = \alpha_m(1 - m) - \beta_m m, \quad \alpha_m = \frac{0.1(V + 40)}{(1 - e^{(V+40)/10})},$$

$$\beta_m = 4 \cdot e^{(-(v+65)/18)}$$

$$\frac{dh}{dt} = \alpha_h(1 - h) - \beta_h h, \quad \alpha_h = 0.07 \cdot e^{-(V+65)/20}.$$

$$\beta_h = \frac{1}{(1 + e^{-(V+35)/10})}$$

The fast delayed rectifier K$^+$ current, I_{Kdr} is given by

$$I_{Kdr} = g_{Kdr}n^4(V - E_K) \qquad (A33)$$

$$\frac{dn}{dt} = \alpha_n(1 - n) - \beta_n n, \quad \alpha_n = \frac{0.01(V + 55)}{(1 - e^{-(V+55)/10})}, \quad \beta_n = 0.125e^{-(v+65)/80}$$

The ionic parameter values are depicted in Table A4.

OLM Cell

$$C_m \frac{dV}{dt} = I_L + I_{Na} + I_{K_{dr}} + I_{NaP} + I_H + I_{syn} + I_{in} \qquad (A34)$$

where C_m is the membrane capacitance, V is the membrane potential, I_L is the leak current, I_{Na} is the sodium current, I_{Kdr}

TABLE A4. ━━━━━━━━

Inhibitory Cell Parameter Values

Name	Value	Name	Value
C_m	1	$g_{K,dr}$	23
g_L	0.18	$g_{K,dr,OLM}$	36
V_L	−60	$V_{k,OLM}$	−77
g_{Na}	150	V_k	−90
$g_{Na,OLM}$	120	g_{NaP}	2.5
V_{Na}	55	g_h	1.5
$V_{Na,OLM}$	50	V_{NaP}	50
$g_{L,OLM}$	0.3	V_h	−20
$V_{L,OLM}$	−54.4	g_A	10

Units: g, mS/cm^2; C_m, μF/cm^2; V, mV.

is the fast delayed rectifier K^+ current, I_{NaP} is the persistent sodium current, I_h is the H-current and I_{syn} is the synaptic current.

The sodium current and its kinetics are described by,

$$I_{Na} = g_{Na}m^3h(V - E_{Na}) \tag{A35}$$

$$\frac{dm}{dt} = \alpha_m(1-m) - \beta_m m, \quad \alpha_m = \frac{0.1(V+40)}{(1-e^{(V+40)/10})},$$
$$\beta_m = 4 \cdot e^{(-(v+65)/18)}$$

$$\frac{dh}{dt} = \alpha_h(1-h) - \beta_h h. \quad \alpha_h = 0.07 \cdot e^{-(V+65)/20},$$
$$\beta_h = \frac{1}{(1 + e^{-(V+35)/10})}$$

The fast delayed rectifier K^+ current, I_{Kdr} is given by
$$I_{Kdr} = g_{Kdr}n^4(V - E_K) \tag{A36}$$

$$\frac{dn}{dt} = \alpha_n(1-n) - \beta_n n, \quad \alpha_n = \frac{0.01(V+55)}{(1-e^{-(V+55)/10})},$$
$$\beta_n = 0.125e^{-(v+65)/80}$$

The NaP current was assembled from the Kunec et al. (2005), Dickson et al. (2000), Fransen et al. (2002, 2004), and White et al. (1998) studies and it was described by

$$I_{NaP} = -g_{NaP} \cdot m_{po} \cdot (V - V_{Na}) \tag{A37}$$

$$\frac{dm_{po}}{dt} = \alpha_{mpo}(V)(1 - m_{po}) - \beta_{mpo}(V) \cdot m_{po}$$

$$\alpha_{mpo} = \frac{1}{0.15(1 + e^{-(V+38)/6.5})}, \quad \beta_{mpo} = \frac{e^{-(V+38)/6.5}}{0.15(1 + e^{-(V+38)/6.5})}$$

Similarly, the h current was assembled from Kunec et al. (2005), Dickson et al. (2000), Fransen et al. (2002, 2004), and White et al. (1998) studies and it was described by

$$I_h = -g_h(0.65\lambda_{fo} + 0.35\lambda_{so})(V - V_h) \tag{A38}$$

$$\frac{d\lambda_{fo}}{dt} = \frac{\lambda_{f\infty}(V) - \lambda_{fo}}{\tau_{\lambda f}(V)}, \quad \lambda_{f\infty}(V) = \frac{1}{(1 + e^{(V+79.2)/9.78})},$$
$$\tau_{\lambda f}(V) = \frac{0.51}{e^{(v-1.7)/10} + e^{-(V+340)/52}} + 1$$

$$\frac{d\lambda_{so}}{dt} = \frac{\lambda_{s\infty}(V) - \lambda_{so}}{\tau_{\lambda s}(V)}, \quad \lambda_{s\infty}(V) = \frac{1}{(1 + e^{(V+2.83)/15.9})^{58}},$$
$$\tau_{\lambda s}(V) = \frac{5.6}{e^{(v-1.7)/14} + e^{-(V+260)/43}} + 1$$

The ionic parameter values are depicted in Table A4.

Hippocampus

Input-to-Cell Synaptic Currents

The Ca^{2+}-NMDA, AMPA, $GABA_A$, and NMDA synaptic currents are given by
$$I_{Ca,NMDA} = -g_{syn} \cdot s_{NMDA} \cdot m_{Ca,NMDA} \cdot (V_d - V_{Ca,NMDA}) \tag{A39}$$

$$I_{NMDA} = -g_{syn} \cdot s_{NMDA} \cdot m_{NMDA} \cdot (V_d - V_{NMDA}) \tag{A40}$$

$$I_{AMPA} = -g_{syn} \cdot s_{AMPA} \cdot (V_d - V_{AMPA}) \tag{A41}$$

$$I_{GABA} = -g_{syn} \cdot s_{GABA} \cdot (V_d - V_{GABA}) \tag{A42}$$

where g_{syn} is the synaptic conductance expressed either by Eqs. (A46) or (1–3) and
$$m_{NMDA} = 1/(1 + 0.3 \cdot Mg \cdot \exp(-0.062 \cdot V_d))$$
$$m_{Ca,NMDA} = 1/(1 + 0.3 \cdot Mg \cdot \exp(-0.124 \cdot V_d))$$

with Mg^{2+} = 2 mM. The activation equations for AMPA, NMDA, and $GABA_A$ currents are
$$s_x = s_{x_{fast}} + s_{x_{slow}} + s_{x_{rise}} \tag{A43}$$

where x stands for AMPA, NMDA, GABA and

$$s'_{NMDA_{rise}} = -20 \cdot (1 - s_{NMDA_{fast}} - s_{NMDA_{slow}}) \cdot F_{pre} - (1/2) \cdot s_{NMDA_{rise}}$$
$$s'_{NMDA_{fast}} = 20 \cdot (0.527 - s_{NMDA_{fast}}) \cdot F_{pre} - (1/10) \cdot s_{NMDA_{fast}}$$
$$s'_{NMDA_{slow}} = 20 \cdot (0.473 - s_{NMDA_{slow}}) \cdot F_{pre} - (1/45) \cdot s_{NMDA_{slow}}$$
$$s'_{AMPA_{rise}} = -20 \cdot (1 - s_{AMPA_{fast}} - s_{AMPA_{slow}}) \cdot F_{pre} - (1/0.58) \cdot s_{AMPA_{rise}}$$
$$s'_{AMPA_{fast}} = 20 \cdot (0.903 - s_{AMPA_{fast}}) \cdot F_{pre} - (1/7.6) \cdot s_{AMPA_{fast}}$$
$$s'_{AMPA_{slow}} = 20 \cdot (0.097 - s_{AMPA_{slow}}) \cdot F_{pre} - (1/25.69) \cdot s_{AMPA_{slow}}$$

and
$$s'_{GABA_{rise}} = -20 \cdot (1 - s_{GABA_{fast}} - s_{GABA_{slow}}) \cdot F_{pre} - (1/1.18) \cdot s_{GABA_{rise}}$$
$$s'_{GABA_{fast}} = 20 \cdot (0.803 - s_{GABA_{fast}}) \cdot F_{pre} - (1/8.5) \cdot s_{GABA_{fast}}$$
$$s'_{GABA_{slow}} = 20 \cdot (0.197 - s_{GABA_{slow}}) \cdot F_{pre} - (1/30.01) \cdot s_{GABA_{slow}}$$

where F_{pre} is the input spike generator simulating the CA3 Schaffer collateral, the EC perforant path and the MS inputs. The input-to-cell synaptic parameter values are displayed in Table A5.

TABLE A5.

Input-to-cell and cell-to-cell synaptic parameter values

Name	Value	Name	Value
$g_{Ca,NMDA}$	25	$V_{Ca,NMDA}$	140
g_{NMDA}	0.3	V_{NMDA}	0
g_{AMPA}	0.05	V_{AMPA}	0
g_{GABA}	0.05	V_{GABA}	−75

Units: g, mS/cm^2; V, mV.

Cell-to-Cell Synaptic Parameter Values

Name	Value	Name	Value
α_{AAC2PC}	5	β_{AAC2PC}	0.01
α_{BC2PC}	5	β_{BC2PC}	0.015
α_{BSC2PC}	5	β_{BSC2PC}	0.01
α_{OLM2PC}	5	β_{OLM2PC}	0.01
α_{IVY2PC}	1	β_{IVY2PC}	0.0015
α_{BC2BC}	3.5	β_{BC2BC}	0.18
α_{BC2BSC}	3.5	β_{BC2BSC}	0.18
α_{BSC2BC}	3.5	β_{BSC2BC}	0.18
α_{NGL2PC}	5	β_{NGL2PC}	0.015
α_{PC2BC}	20	β_{PC2BC}	0.19
α_{PC2BSC}	20	β_{PC2BSC}	0.19
α_{PC2AAC}	20	β_{PC2AAC}	0.19
α_{PC2IVY}	20	β_{PC2IVY}	0.19
α_{PC2OLM}	20	β_{PC2OLM}	0.19
$\alpha_{OLM2NGL}$	5	$\beta_{OLM2NGL}$	0.01

Units: g, mS/cm^2; V, mV; α, 1/ms; β, 1/ms.

Input Spike Generator

The input spike generator simulating the CA3 Schaffer collateral, the EC perforant path, and the MS inputs were described by

$$F_{pre} = H(t - 1) \cdot (H(\sin(2\pi \cdot (t - 2)/T)) \cdot (1 - H(\sin(2\pi \cdot (t - 1)/T)))) \tag{A44}$$

where T is the period of oscillation and $H(\bullet)$ is the Heaviside function.

Cell-to-Cell Synaptic Currents

The synaptic current is given by
$$I_{syn} = g_{syn} \cdot s \cdot (V - E_{rev}) \tag{A45}$$

where g_{syn} is the synaptic conductance and E_{rev} is the reversal potential. The synaptic conductance is expressed by
$$g_{syn} = w \cdot DA \cdot g_{max} \tag{A46}$$

where g_{max} is the maximal synaptic conductance, DA is the dopamine level, and w is the synaptic strength. The DA level is always 1 unless mentioned otherwise. The values of the synaptic strengths are given in Table A1. In the model three synaptic currents are included: AMPA, NMDA, and GABA$_A$. The values of the synaptic parameters are displayed in Table A5. The gating variable, s, which represents the fraction of the open synaptic ion channels, obeys the following differential equation

$$\frac{ds}{dt} = \alpha \cdot F(V_{pre}) \cdot (1 - s) - \beta \cdot s \tag{A47}$$

where the normalized concentration of the postsynaptic transmitter-receptor complex, $F(V_{pre})$, is assumed to be an instantaneous and sigmoid functions of the presynaptic membrane potential

$$F(V_{pre}) = 1/(1 + e^{-(V_{pre}-\theta)/2}) \tag{A48}$$

where $\theta = 0$ mV is high enough so that the transmitter release occurs only when the presynaptic cell emits a spike (Cutsuridis et al., 2007). The values of the channel opening and closing rates are displayed in Table A6.

Pyramidal Cell

Axonic (a) and somatic (s) compartments receive GABA$_A$ inhibition from axo-axonic and basket cells, respectively. The proximal dendritic (pd) compartment receives both AMPA and NMDA excitation from the CA3 Schaffer collateral input and GABA$_A$ inhibition from the bistratified and ivy cells. The distal dendritic (dd) compartment receives AMPA and NMDA excitation from the EC perforant path and GABA$_A$ inhibition from the neurogliaform and OLM cells. Both pd and dd AMPA and NMDA synapses are plastic and change according to the Eqs. (1)–(3).

Axo-Axonic and Basket Cells

The somatic (s) compartments of both axo-axonic and basket cells receive AMPA excitation from both the EC perforant and the CA3 Schaffer collateral paths. Axo-axonic cells receive also GABA$_A$ inhibition from the medial septal cells. Basket cells receive GABA$_A$ inhibition from the bistratified cells and the medial septal cells.

Bistratified Cells

The somatic (s) compartment of the bistratifed cells receive AMPA excitation only from the CA3 Schaffer collateral path and GABA$_A$ inhibition from the basket cells and the medial septal cells.

OLM, Neurogliaform, and IVY Cells

The IVY cells receive recurrent AMPA excitation from the pyramidal cells and GABA$_A$ inhibition from the medial septal cells. The neurogliaform cells receive AMPA excitation from the EC peforant path and GABA inhibition from OLM cells, whereas the OLM cells receive AMPA excitation from the pyramidal cells and GABA$_A$ inhibition from the septum.